INVESTIGATION OF NANOPARTICLE DELIVERY TO CANCER CELLS BY CONJUGATION WITH VARIOUS TARGETING MOIETIES

by

LEILA HOSSEIN RASHIDI

Presented to the Faculty of the Graduate School of

The University of Texas at Arlington in Partial Fulfillment

Of the Requirements

For the Degree of

MASTER OF SCIENCE IN BIOENGINEERING

THE UNIVERSITY OF TEXAS AT ARLINGTON

December 2013

Acknowledgements

Firstly, I would like to sincerely thank my advisor Professor Wei Chen for his guidance and support as well as entrusting me with the responsibility of many exciting and challenging research projects to work on which helped me improve my research and analytical skills tremendously. It was my great pleasure and honor to have the opportunity to work with him.

Also, my sincere gratitude to Professor Kytai Nguyen and Professor Baohong Yuan for serving as committee members and for their time in reviewing my research work as well as all their guidance and suggestions.

I would like to extend my gratitude to Professor Kytai Nguyen for permitting us to use some instruments in their lab, Professor Jer-Tsong Hsieh in UT Southwestern Medical Center and Professor Richard Timmons at UT Arlington, Department of Chemistry and Biochemistry, for providing us with some of the materials.

Also my deepest gratitude to our lab's previous research scientist fellow, Dr. Xiaoju Zou and Dr. Li Liu in UT Southwestern Medical Center, for helping me with cell studies and also for explaining and discussing many issues that I came across during my research. I would like to thank all the members in nano-bio physics group, especially my heartfelt thanks to Dr. Homa Homayoni who generously shared her knowledge with me from the initial steps of my research experience.

I am also very grateful to my Husband, Mojtaba, for his endless love, support, and encouragement.

Lastly but not the least, I wish to extend my utmost heartfelt appreciation to my family for their endless love, encouragement, and support. They have always been the great source of inspiration to me.

November 11, 2013

Abstract

INVESTIGATION OF NANOPARTICLE DELIVERY

TO CANCER CELLS BY CONJUGATION

WITH VAROIUS TARGETING

MOEITIES

Leila Hossein Rashidi (M.S.)

The University of Texas at Arlington, 2013

Supervising Professor: Wei Chen

Recently, mapping and profiling of specific tumor biomarkers characterizing cancer cells, followed by understanding of signal cascades involved in the pathogenesis of tumors (targeted therapy), as well as diagnosis in early stages, have become promising topics in cancer research. Since, the most considerable limitations of conventional therapies and diagnostic modalities are associated with nonspecific targeting; designing intelligent new anti-cancer nanocarries improved by targeting biomolecules could enhance therapeutic efficiencies as well as diagnosis in early stage of cancer. Active targeting which is based on the surface accessibility and the high level of expression of specific cancer antigens has attracted much attention in the last decade, since it could result in highly efficient treatments and markedly reduced systemic toxicities. In this study two different nanoparticles (NPs) synthesized in this lab were used in order to conjugate with variety of biomolecules to investigate cancer cells targeting. Firstly, $Sr_3MgSi_2O_8:Eu^{2+}$, Dy^{3+} persistent luminescence NPs were conjugated to folic acid (FA) through a simple EDC/NHS (1-Ethyl-3-(3-dimethylaminopropyl) carbodiimide /N-hydroxysuccinimide) chemistry. Then, some characterization studies were conducted.

The luminescent properties of the NPs after conjugation were studied. UV-Vis Absorption spectra was used to confirm conjugation, as well as calculating the conjugation efficiency. Zeta potential was performed using dynamic light scattering (DLS) device to confirm the FA conjugation to NPs. The size of NPs after conjugation was measured using DLS. Cell viability studies were done using MTT assay (3-(4,5-dimethylthiazol-2-yl)-2,5-diphenyltetrazolium bromide). Finally fluorescent imaging was done using PC-3 cells (negative for folic acid), MCF-7 (positive for folic acid), and KB cells (positive for folic acid) to compare the cellular uptake and confirm targeted delivery. These persistent luminescence NPs could be further conjugated with photosensitizer so they can be used for targeted photodynamic therapy especially for breast cancer cells. Also the same NPs were conjugated to cyclic RGDfK and fluorescent imaging was carried out using MDA-MB-231 breast cancer cell line as positive for $\alpha_v\beta_3$ integrin receptor and MCF-7 as negative for $\alpha_v\beta_3$ integrin receptor to compare the cellular uptake and confirm targeted delivery. The main reason for choosing RGD peptide over folic acid was the more specificity of RGD peptide to breast cancer cells as compared to folic acid. Moreover, the ZnS:Mn luminescent NPs were used to conjugate to prostate specific membrane antigen (PSMA) inhibitor. It has been shown that inhibitors of PSMA strongly bind to PSMA expressed on prostate cancer cells. LNCaP and PC-3 cell lines were used as positive and negative for PSMA receptors in fluorescent imaging to compare the cellular uptake and confirm targeted delivery. Finally, the persistent luminescence NPs were conjugated to R11-SH peptide and fluorescent Imaging was performed on LNCaP and PC-3 cells as models for prostate cancer cell lines and the uptake was studied. Consequently, based on all the results related to different biomolecules, cellular uptake and targeting of luminescent NPs could be enhanced, by conjugation to variety of biomolecules, which are specific for breast and prostate cancer cells, in a receptor dependent manner.

Table of Contents

List of Illustrations

List of Tables

Chapter 1

Introduction

1.1 Cancer, Challenges and Possible Solutions

Cancer has one of the highest mortality rates worldwide and is the second leading cause of death after heart disease, in the United States and is responsible for 25% of deaths overall. [1, 2] The burden of cancer involves the affected patients and their loved ones, who suffer physically, emotionally and financially, as well as society in general through increased healthcare burdens on hospitals and employment disruption. Due to higher incidence rates among the elderly and middle-aged and the fact that the population is living longer than ever before, the overall costs to society will most likely continue to grow in the near future. A potent solution to the personal and societal burden is the early detection of cancer in a preclinical stage before tumor cells metastasize, which will prevent patient suffering, garner better therapeutic outcomes, and present fewer costs to the patient and their communities [2, 3]

A great number of cancers could be effectively treated resulting in patient's full recovery, if they could be detected at early stage. However, early stage diagnosis followed by therapy have been remained a significant challenge, since clinical symptoms are not usually clear until cancer progresses to a fetal stage. In addition, current diagnostic and therapeutic approaches are mostly invasive (i.e. random biopsies and surgery) as well as crude, nonspecific methods (i.e. irradiation and chemotherapeutic agents). Thus, these therapeutic techniques are in urgent need to be improved and replaced by minimally invasive, user friendly technologies for efficient detection and prognosis of cancer. Recently, varieties of nanoparticulate-based devices have been introduced for improved diagnostic imaging and therapy of many types of cancers, as

well as targeted delivery of those systems carrying chemotherapeutic drugs. Targeted drug delivery could minimize radiation and drug dose, as well as replacing the invasive surgery. In addition more sensitive imaging techniques could be incorporated for earlier detection and better prognosis resulting in improved cancer treatment [2, 3, 4]

1.1.1 Nanotechnology for Cancer Detection and Treatment

Nanomedicine involves the use of nanotechnology in the collective or stand-alone treatment and detection of diseases that benefit from observation on the nanoscale, such as cancer. Nanoparticles range from 1–100 nm in diameter and are therefore attractive as therapeutic and imaging agents in oncology because of their small size and also the unique physical and chemical properties innately associated with them. Nanoparticles clearly are smaller than biological organelles but are similar in dimensions to biological macromolecules, making them desirable for micro-scale and submicron engineering. They also possess a high surface area-to-volume ratio which allows potential cargo loading (i.e. chemotherapeutic drugs, plasmid DNA and siRNA) and have customizable surface chemistries for targeting of specific cell or marker types. Specifically for cancer, nanoparticles between 10 and 100 nm in size preferentially could gather at tumor sites due to the enhanced permeability and retention (EPR) effect, through passive targeting, making them advantageous for targeting even without specified moieties. Therefore, nanoparticles possess advantages and properties which give them potential applications in early detection through enhanced imaging, therapies or even combined imaging and therapy called “theranostics” due to their highly customizable chemical nature. Nanoparticles can be created using organic molecule building blocks for drug and gene delivery (i.e. liposomes, polymeric constructs, polymeric micelles and polymeric nanoparticles), or using inorganic building blocks to obtain unique properties including magnetic control or noble metal thermal ablation.

However, optical, magnetic, and other physical properties, as well as inertness, stability, and ease of functionalization, have made inorganic nanoparticles very promising alternatives to organic nanoparticles for imaging and ablation of malignant tissue. The most-studied of the common inorganic nanoparticles are gold, semiconductor fluorescent quantum dots, upconversion luminescence and magnetic nanoparticles. [1, 2]

1.1.1.1 Cancer Detection Using Nanoparticles

Nanoparticles are widely used as probes for in-vivo imaging, bio-sensing, and immune-staining, since they have introduced many advantages. Firstly, varieties of nanoscale materials show unique magnetic, optical, or acoustic properties and they can be further combined with other types of imaging functionalities resulting in novel probes with multimodal capabilities. Thus, they could offer high sensitivity compared to other devices. Secondly, their size is usually in a desired range for biomedical applications. A great number of nanoparticles have a size that is above the threshold of renal clearance (<7 nm) allowing them to remain in circulation for a relatively long time before reaching the desired targets. This could result in higher uptake by target cells which may lead to higher imaging and detection efficiencies. In addition, because of their small enough size, they can readily penetrate into many biological barriers such as endothelial barriers, cell membranes, or even nuclear envelopes to efficiently interact with biological systems on the molecular level. Thirdly, they are multivalent, so that multiple targeting ligands can be conjugated onto nanoparticles surface. Consequently, larger rate of receptor binding and smaller rate of dissociation, could lead to higher tumor uptake and longer retention time, which is known as multivalency effect. Therefore, more sensitive and specific imaging modalities could be achieved. On the other hand, it is possible to conjugate more than one type of targeting ligand as confirmed by recent studies. Fourthly, they can be used as both imaging probes and therapeutic devices. [1, 4]

Considering all these advantages for nanoparticles, especially inorganic nanoparticles, many different kinds of nanoparticles with variety of properties for cancer detection have been introduced in the following. An ideal detection system would accumulate all the advantages of each type of nanoparticles and reduce their respective disadvantages as much as possible.

1.1.1.1.1 Magnetic Nanoparticles for Cancer Diagnosis: Magnetic nanoparticles have been widely used in biomedical applications such as contrast probes for magnetic resonance imaging (MRI). Magnetic nanoparticles create microscopic field gradients in a strong magnetic field which could cause shortening and diphase of longitudinal (T1) or transverse relaxation times (T2 and T2*) of nearby nuclei (i.e. protons). This induces hyper- (for T1) or hypo-intensities (for T2 and T2*) on MRI maps which leads to highlighting the areas that are concentrated with the particles. Magnetic nanoparticles, especially iron oxide nanoparticles (IONPs) and super paramagnetic iron-oxide nanoparticles (SPIOs) are extensively used in liver imaging, lymph node imaging, cell tracking and most commonly, as contrast agents for MRI. [1, 2, 4]

1.1.1.1.2 Quantum Dots for Cancer Diagnosis: Optical fluorescence imaging is widely used in tumor diagnosis, especially in preclinical stage. By incorporating small animal whole-body, fluorescence imaging systems could be a sensitive and cost-effective tool in preclinical cancer studies, biomarker discovery and drug development. Fluorescence imaging has been extensively used in immune-staining field for analyzing patient samples and also at endoscopic and intraoperative settings. The only limitation accounts for fluorescence imaging, is when deep tissue penetration is a concern, especially for cancer diagnostic and imaging. Light transmission is severely attenuated when traveling both in and out of tissues because of all the scatterings and absorptions which could lead to a shallow penetration depth (typically less than 1 cm). A possible solution for this limitation

is using fluorophores with absorption and emission in the near infrared region can reduce the energy loss to some extent. However, in vivo fluorescence imaging has been limited to subcutaneous models or targets close to the skin. Recently, inorganic nanoparticle based fluorophores have been found to offer promising advantages over traditional organic dyes. Among all, quantum dots (QDs), which are semiconductor nanoparticles composed of groups II and VI elements (i.e. CdSe and CdTe) or groups III and V elements (e.g. InP and InAs), have been widely studied. Unlike bulk quantum dots which mostly behave like insulators at ambient conditions, QDs, have a physical size of 2–10 nm in diameter, which is smaller than the exciton Bohr radius. This results in a three dimensional quantum confinement of charge carriers, limiting the number of possible energy states that an electron can occupy. Thus, usually relaxation of an excited electron in QDs results in the release of the band gap energy in the form of light in the visible or near-infrared (NIR) region which has the benefit of unique absorption and emission profiles. QDs could yield a broad absorption spectrum but a narrow and usually symmetrical sharpness of the luminescent peak as compared to organic fluorophores which exhibit an emission spectrum that is usually a mirror image of the absorption one. Consequently, QDs could offer promising properties, most importantly offering deep tissue penetration, making them alternative candidates for optical imaging in cancer diagnosis field. [1, 2, 4]

1.1.1.1.3 Upconversion Nanoparticles for Cancer Diagnosis: Upconversion nanoparticles (UCNPs) have recently attracted much attention in optical imaging field. UCNPs absorb NIR light (~980 nm) and emit with higher frequency. The anti-Stokes shift is caused by a nonlinear optical process in which two or more photons are almost simultaneously absorbed to provide sufficient energy for the upconversion. UCNPs show a much lower “Quantum Yield” than QDs in the range of 0.005–0.3, with the highest measured value

being 0.3% for 100 nm $NaYF_4$: Yb^{3+}, Er^{3+} nanoparticles. UCNPs imaging has the advantage of clean background. As a result, for in vivo imaging, this property may lead to an increased signal-to-noise ratio and longer penetration depth. Thus, these UCNPs nanoparticles have been a promising candidate for optical imaging in cancer diagnosis. [4]

1.1.1.1.4 Gold Nanoparticles for Cancer Diagnosis: Recently gold nanoparticles have been extensively used in biomedical applications because of their surface plasmon resonance (SPR) properties which leading to a strong absorption in the visible (and NIR) region. This phenomenon is defined as the collective oscillation of free electrons on the gold particles' surfaces and only occurs when metallic particles have a diameter smaller than the light wavelength. By increasing the size form 5 nm to 9, 22, 48, and 99nm SPR band is red shifted form ~520 nm to 517, 521, 533, and 575 nm. The gold particles' size is found to affect the absorption cross-section as well as light scattering when particles are exposed to electromagnetic radiation. The larger the particle size is, the more light scattering occurs which reduces absorption. For a special application, picking the right nanostructure could be more important because of the size effect. [4] For instance, in optical coherence tomography (OCT), large gold nanoparticles are preferred for stronger scattering and better signal-to-noise contrast. On the other hand, for photothermal therapy applications, relatively small particles are used to have the benefit of their higher absorption efficiency. In addition, when gold nanoparticles aggregate, plasmon–plasmon interaction occurs, leading to a substantial color change from red to blue which could be effectively used in colorimetric detection methods. Moreover, geometry of the gold nanoparticles also has a large impact on the SPR. By changing the length-to-diameter ratio of the gold nanoparticles, it is possible to achieve a longitudinal plasmon band that matches commercial lasers at 360, 785, and 1064. Also, the absorption is determined by

the ratio of the thickness to diameter of the cavity. The smaller the ratio, the further the plasmon absorption shifts to the NIR region. [4]

Considering all the properties of gold nanoparticles mentioned above, they can also be used in two-photon luminescent (TPL) imaging which is a potential diagnostic technique for precancerous and cancerous epithelial tissues. However the penetration depth is limited to the use of NIR light. In TPL imaging, two photons at the same lower energy, comparable to a single photon at high energy, can be employed to excite electrons in noble metals (i.e. gold and silver); the TPL signal from a metallic nanoparticle can be greatly enhanced due to localized surface plasmon resonance. The NIR longitudinal band of gold nanorods overlaps with TPL excitation spectrum, so that these nanoparticles could be ideal probes for TPL-based imaging of tissue. Moreover, Photoacoustic tomography (PAT) is a hybrid imaging technique which combines the both light and ultrasound-based imaging. PAT could provide the optical contrast of an object 5 cm deep in biological tissue, which is almost the deepest range introduced recently, with a high spatial resolution of approximately 0.2 mm. PAT works by detecting ultrasonic waves which are induced by pulsed laser exposure of biological tissue. Thus, gold nanoparticles have been investigated as contrast enhancement agents for PAT, since they are not sensitive to photobleaching and are able to create higher levels of photoacoustic signals in the NIR. [1, 4]

1.1.1.2 Cancer Treatment Using Nanoparticles

There are variety of cancer therapies which are all used in recent years, such as surgery, hormone therapy, immune therapy, chemotherapy, radiation therapy, phototheraml therapy and photodynamic therapy. Herein, chemotherapy, radiation therapy, photothermal therapy and photodynamic therapy were discussed as they are the most common methods using nanoparticles.

1.1.1.2.1 Chemotherapy: The major therapeutic approach for the treatment of localized and metastasized cancer is chemotherapy, which is used alone or combination with other forms of therapy. However, conventional chemotherapy has some limitations such as (a) Limited aqueous solubility (b) Lack of selectivity of anticancer drugs (c) Multidrug resistance (MDR). To overcome the limitation of conventional oral dosage form in many therapeutic areas particularly in cancer chemotherapy, recently, nanoparticulate drug delivery systems have been introduced. Multidrug resistance, which is the major problem in cancer chemotherapy, can be effectively overcome by incorporating Mesoporous Silica Nanoparticles, Solid lipid nanoparticles, Polymeric nanoparticles and Magnetic nanoparticles. Moreover, poor aqueous solubility and low bioavailability of cancer chemotherapeutic can be effectively circumvented by nanocrystals, albumin based nanoparticles, liposomal formulation, Polymeric micelles, cyclodextrin and chitosan based nanoparticles. [5]

However there are still many problems using chemotherapy alone. Some of the disadvantages of chemotherapy include systemic toxicities are hair loss, weakness, immuno-suppression, and weight loss. [2, 6] Other methods which could effectively be combined with chemotherapy to reduce the drug dose and side effects are highly encouraged.

1.1.1.2.2 Radiation Therapy: Radiotherapy is still the most common and efficient cancer treatment since 1896. Principle of radiotherapy of cancer is its irradiation with high-energy radiation to destroy malignant cells in a treated volume. It was shown that radiation treatment of both glioma and prostate cancer requires high accuracy in delivering ionizing radiation to minimize toxicity to normal surrounding tissues. Metallic nanoparticles could enhance the therapeutic efficiency of radiotherapy by selectively scattering and/or absorbing X-rays and gamma rays causing localized damage to DNA

and other targeted organelles of cancer cells. Therefore, nanoparticulate systems could contribute to decreasing total radiation dose to minimize side effects of ionizing radiation on cancer patients. Also Quantum dots and some of the nanoparticles could be potential candidates for radiation therapy (i.e. ZnS, ZnO, LaF, CaF, silicon nanoparticles). [7]

However Radiation therapy could cause many side effects such as tiredness, diarrhea, uncomfortable urination, and hair loss in the pelvic area. [2, 6] Other methods which alone or in combination with previous therapies could reduce these therapies side effects are highly encouraged. Herein, photothermal and photodynamic therapy were introduced, which have attracted much attention in recent years because of their less harmful nature.

1.1.1.2.3 Thermal ablation and Photothermal Therapy

1.1.1.2.3.1 Magnetic Nanoparticles for Thermal Ablation Therapy: In addition to widespread use of magnetic nanoparticles in cancer diagnosis and imaging, super paramagnetic iron oxide nanoparticles (SPIOs) have the potential for use as ablation agents to thermally treat cancer since tumor cells are more vulnerable to heat than normal cells. SPIOs convert electromagnetic energy into heat when they are subjected to an alternating magnetic field, followed by dissipating the heat to the surrounding medium. However, Targeted nanoparticulate systems are required for selective uptake by tumor cells in SPIO-mediated tumor ablation. In order to prevent local heating and damage of normal tissues, both the tissue distribution of SPIOs prior to heating treatment as well as the temperature evolution during hyperthermia should be monitored. Thus, these nanoparticles are promising candidates for combined diagnosis and thermal therapy, since MRI can be used to monitor the tissue distribution as well as local temperature change because of to the temperature dependence of proton relaxation times. [1]

1.1.1.2.3.2 Gold Nanoparticles for Photothermal Therapy: As discussed in previous part, thermal therapy is an effective therapeutic modality for the ablation of tumors especially in combination with conventional treatments (i.e. surgery, chemotherapy, and radiation therapy). The most advantageous point of recent modalities is the ability to generate hyperthermic temperatures (>43 °C) at a desired site with externally tunable control in comparison to whole-body hyperthermia. Photothermal and radio-frequency (RF)-based thermal treatments using immunotargeted gold nanoparticles, including nanospheres, nanorods, nanoshells, nanoclusters, and nanocages have shown promising results with the ability to selectively induce cancer cell damage via hyperthermia, while minimally affecting non-targeted cells. [1]

Radio frequency (RF) radiation of gold nanosphres, which has deeper penetration in vivo have attracted much attention in order to induce thermal ablation of tumors, as compared to photothermal activation, which uses visible light (~520 nm), resulting in limited applications to superficial malignancies, due to restricted tissue penetration depth of visible light. Cylindrical gold nanorods and gold nanoshells consisting of an ultrathin gold shell surrounding a dielectric core (e.g. silica) demonstrated a tunable photothermal response to near infrared (NIR) light. [1]

1.1.1.2.4 Photodynamic Therapy: Recently, photodynamic therapy has attracted much attention as a promising therapeutic option for cancer and other diseases. PDT incorporates light-sensitive drugs or photosensitizers (PS) that can be preferentially localized in malignant tissues. This therapeutic effect could be achieved by photo-excitation of the localized photosensitizer to generate a cytotoxic species, (i.e. singlet oxygen ($^1O_2$), free radicals, or peroxides). This could result in selective and irreversible destruction of diseased tissues (i.e. cancerous tissues), without damaging healthy cells and tissues. Another important advantage of PDT as compared to conventional methods

for cancer therapy such as radiotherapy and chemotherapy or prolonged hospitalization of surgery is outpatient therapeutic property of PDT. Moreover, PDT can induce immunity, even against less immunogenic tumors, resulting in long-term tumor control. Even though PDT has recently gained much attention because of the above mentioned advantages, it still needs to gain general clinical acceptance. In the following, some of the technical problems of PDT are discussed. Firstly, currently FDA approved PDT photosensitizers absorb light just in the visible spectral regions (below 700 nm), where light penetration into the skin is only a few millimeters, leading to limited PDT application for treating relatively superficial lesions. However, availability of advanced fibre-optic scopes which can reach most body cavities could be a possible solution for this problem. Secondly, most existing photosensitizers are hydrophobic and aggregate easily under physiological condition. So designing a nanoparticluate-based delivery system is highly encouraged. Thirdly, they do not offer high enough accumulation selectivity to diseased tissues for clinical use. Thus, as discussed above, designing novel nanoparticulate systems could offer solutions to these difficulties which are summarized in the following. [8]

1.1.1.2.4.1 Photosensitizer Nanoparticles for Photodynamic Therapy: Quantum dots (QDs) are nanoparticulate imaging probes with high quantum yields, high photo-stability and fluorescent emission properties which can be tuned by changing the size. They can be exhibit water solubility properties by different choice of synthesis methods and be targeted to specific pathological areas. QDs can transfer energy to surrounding O_2, resulting in toxicity to cells. [8] Figure 1-1 is the schematic representation of photosensitizer nanoparticles.

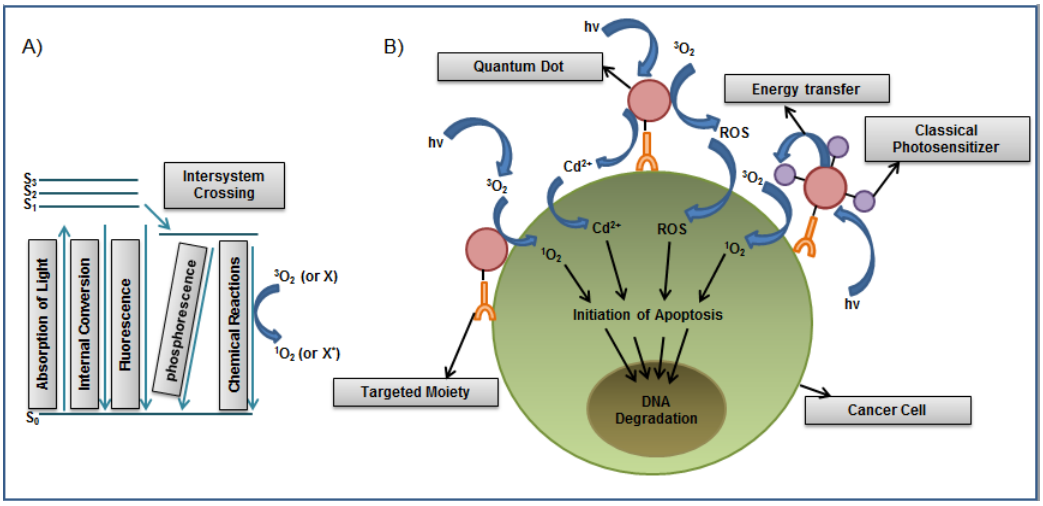

Figure 1-1 Nanoparticles as possible photosensitizers: A) Photodynamic processes involved in photodynamic therapy. B) Possible mechanisms of photodynamic processes by quantum dots [8]

1.1.1.2.4.2 Persistent Luminescence Nanoparticles for Photodynamic Therapy: There is a new approach to cancer treatment through a combination of radiation therapy and PDT which they have named Self Lighting Photodynamic Therapy (SLPDT). Under this concept, scintillation or persistent luminescence nanoparticles conjugated with photosensitizers (i.e. porphyrin) are used as in vivo agents for PDT. Upon exposure to ionizing radiation such as X-rays, nanoparticles emit luminescence which activates the photosensitizers; consequently, singlet oxygen is produced to kill cancer cells along ionizing radiation. Thus, conventional radiation therapy could be combined with PDT which enables the use of lower doses of radiation. [8] Figure 1-2 illustrates the mechanism of PDT for persistent lumuninescence nanoparticles, so called afterglow nanoparticles (AG NPs), conjugated to a photosensitizer (porphyrin), targeted through folic acid conjugation, to cancer cells, followed by effective and specific killing of those cells.

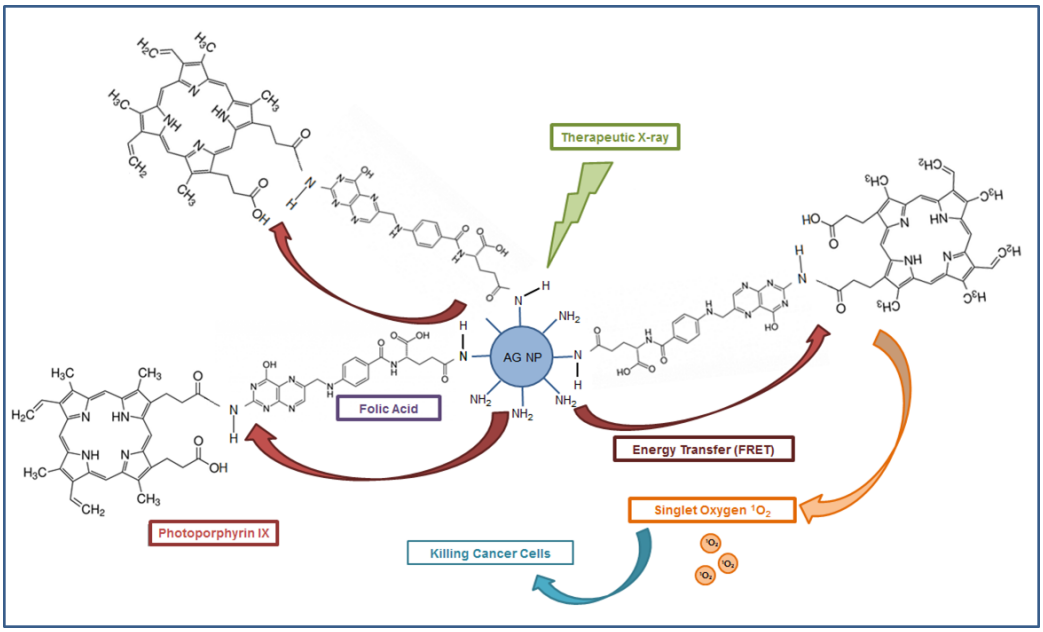

Figure 1-2 Schematic representation of the nanoparticle-based X-ray-induced photodynamic therapy: Under ionizing radiation a nanoparticle starts to scintillate transferring its energy into a conjugated porphyrin molecule, which then generates singlet oxygen necessary to produce photosensitizing effect. This methodology will help to treat nodular and deeper tumors due to higher penetrating capacity of X-rays and gamma rays compared to that of visible light commonly used in PDT. [7]

1.1.1.2.4.3 Upconversion Luminescence Nanoparticles for Photodynamic Therapy: Upconvesion nanoparticles (UCNPs) are synthesized by using the transition metal, lanthanide, or actinide ions doped into a solid-state host and generate higher energy light from lower energy radiation, usually near-infrared (NIR) or infrared (IR). There are several advantages for using upconversion nanoparticles in photodynamic field. Firstly, optical absorption coefficients of principal tissue chromophores in the human body show a very sharp ‘valley’ in the NIR region, so that deepest tissue penetration could occur, since NIR light can penetrate much higher than visible light into tissue layers as well as

less harmful influence of NIR light on adjunct healthy tissues. In addition, nanoparticles may effectively accumulate in tumors due to an enhanced permeation and retention effect, which could be caused by disordered tissue architecture, increased vascularity, larger microvascular fenestrations and absence of lymphatics (passive targeting). Moreover, this specificity could be improved by other targeting molecules attached to the surface (active targeting). NIR light can penetrate to a considerable extent in soft fibro-fatty tissues like the breast, thus, the upconversion nanoparticles can potentially be used for both therapy and monitoring of tumors over time.

To use these nanoparticles for photodynamic therapy, zinc pthalocyanine (ZnPC) photosensitizer were attached to the surface of the nanoparticles. For instance, incident NIR laser light is upconverted by the nanoparticles to red light, which is used by the photosensitizer ZnPC to produce singlet oxygen species from dissolved molecular oxygen in the micro-environment. The nanoparticles contribute to three different roles which could benefit the results. Firstly, it helps to solubilize the highly non-polar ZnPC which tends to aggregate in aqueous solutions. Secondly, it helps to convert low energy light to the higher energy radiation which is necessary to excite the ZnPC. Finally, the nanoparticles help to target the ZnPC to cancer cells. [8]

1.1.1.2.4.4 Gold Nanoparticles for Photodynamic Therapy: Metallic nanoparticles are known to be effective fluorescent quenchers. However, it has been shown recently that fluorescence intensity can be enhanced by plasmonic nanoparticles (i.e. Ag and Au) if the molecules are placed at an optimal distance from the metal. Consequently, this could improve the effectiveness of PDT. [9] In a recent study, pegylated gold nanoparticle silicon phthalocyanine (AuNp-Pc4) conjugates have been developed as efficient drug vectors for PDT drug delivery. AuNp-Pc4 conjugates are water-soluble and biocompatible

nanoparticles which showed significant enhancement in the delivery of the PS to the tumor site compared to conventional administration of photosensitizers. [10, 11]

1.2 Targeting Strategies

One of the most considerable limitations of conventional treatments and diagnosis procedures is associated with non-specific targeting of therapeutic and diagnosis modalities. Targeted therapy and diagnosis with cancer specificity could be an alternative modality which could enhance therapeutic efficacy for patients as well as diagnosis in early stage of cancer. [6]

In cancer therapy, the tumor microenvironment allows researchers to introduce and study different therapeutic strategies, based on differences of diseased tissue as compared with normal tissue, including vascular abnormalities, oxygenation, perfusion, pH and metabolic states. Tumor vasculature and the pH will be are more relevant characteristics for the design of nanoparticulate systems as tumor targeted drug delivery systems and are discussed in the following.[12]

1) Angiogenesis in cancer:

Formation of new blood vessels from existing ones is called angiogenesis. For solid tumors (1–2 mm^3), the mechanism of reaching oxygen and nutrients to the center of the tumor is via simple diffusion. Non-angiogenic tumors are highly dependent on their microenvironment for oxygen and the supply of nutrients because of their non-functional or non-existent vasculature. When tumors reach 2 mm^3 in size, a state of cellular hypoxia begins, resulting in initiating angiogenesis. The balance of some activators and inhibitors could regulate the angiogenesis. There are five main phases in the angiogenesis process: 1. endothelial cell activation, 2. basement membrane degradation, 3. endothelial cell migration, 4. vessel formation, and 5. angiogenic remodeling. Hypoxia could increase cellular hypoxia inducible factor (HIF) transcription, resulting in upregulation of pro-

angiogenic proteins such as vascular endothelial growth factor (VEGF), platelet derived growth factor (PDGF) or tumor necrosis factor-α (TNF-α). Then, Activated endothelial cells could express the dimeric transmembrane integrin $\alpha_v\beta_3$, which interacts with extracellular matrix proteins (vibronectin, fibronectin, etc.) and regulates the migration of the endothelial cell through the extracellular matrix during vessel formation. In addition, the activated endothelial cells synthesize proteolytic enzymes, such as matrix metalloproteinases, which is used to degrade the basement membrane and the extracellular matrix. Thus, the inner layer of endothelial cells undergoes apoptosis resulting in formation of the vessel lumen. Moreover, immature vasculature undergoes extensive remodeling and during that process the vessels are stabilized by pericytes and smooth-muscle cells. However, this step is often incomplete leading to irregular shaped, dilated and tortuous tumor blood vessels. The ability of angiogenic switch (from non-angiogenic to angiogenic) is the basic of progression of cancer which further allows the dissemination of cancer cells throughout the body, resulting in metastasis. [12, 13]

2) Enhanced Permeability and Retention (EPR) effect:

Long-circulating particulate carrier systems could take the advantage of structural changes in vascular pathophysiology. In some studies, the ability of vascular endothelium to present open fenestrations was described for the sinus endothelium of the liver, when the endothelium is perturbed by inflammatory process, hypoxic areas of infracted myocardiumor in tumors. In addition, tumor blood vessels are usually characterized by abnormalities such as high proportion of proliferating endothelial cells, pericyte deficiency and aberrant basement membrane formation resulting in an enhanced vascular permeability. Nanoparticles, (usually, in the size range of 20–200 nm), can readily extravagate and accumulate inside the interstitial space and also endothelial pores have sizes varying from 10 to 1000 nm. In addition, lymphatic vessels are absent or non-

functional in tumor. This could lead to inefficient drainage from the tumor tissue. Thus, Nanoparticles which have entered into the tumor are not removed efficiently and are retained in the tumor. This passive phenomenon has been called the Enhanced Permeability and Retention (EPR) effect. The abnormal vascular architecture in cancer tissues plays a major role for the EPR effect for selective macromolecular drug targeting. The following summarizes the abnormal vascular architecture role in nanoparticulate systems accumulation which also is illustrated in Figure 1-3.

(1) Extensive angiogenesis and hyper-vasculature

(2) Lack of smooth-muscle layer, pericytes

(3) Defective vascular architecture: fenestrations

(4) No constant blood flow and direction

(5) Inefficient lymphatic drainage that leads to enhanced retention in the interstitium of tumors

(6) Slow venous return that leads to accumulation from the interstitium of tumor

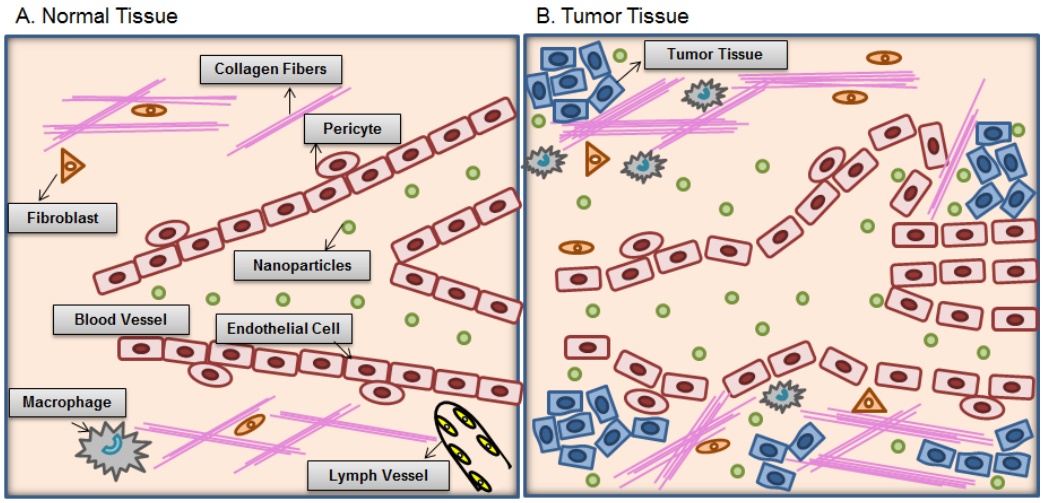

Figure 1-3 Differences between normal and tumor tissues explaining the passive targeting of nanoparticulate systems by the Enhanced Permeability and Retention effect (EPR effect). A. Normal tissues contain linear blood vessels maintained by pericytes. Collagen fibres, fibroblasts and macrophages are in the extracellular matrix. Lymph vessels are present. B. Tumor tissues contain defective blood vessels with many sac-like formations and fenestrations. The extracellular matrix contains more collagen fibres, fibroblasts and macrophages than in normal tissue. Lymph vessels are lacking. [12]

In addition, vascular abnormalities could cause some physiological changes in blood flow within the tumors and in transport properties of tumor. The high tumor interstitial fluid pressure (IFP) could be a barrier for efficient anti-cancer drug delivery. The mechanism of transportation of many anti-cancer drugs (high molecular weight compounds) from circulatory system through the interstitial space is through convection rather than by diffusion. Increased IFP is leading to a decreased transcapillary transport in tumors, resulting in decreased uptake of drugs into tumor. Moreover, IFP is higher at the center of solid tumors, which is decreased toward the periphery, and therefore, creating a mass flow movement of fluid away from the central part of tumor. Drug-loaded

nanoparticulate systems should migrate through the tumor interstitial space from a site of entry to remote cells to have efficient drug supply in the tumor site, but process is hindered by high IFP. The transport of nanoparticulate systems is less affected by this enhanced IFP in tumors because of the larger size of those nanoparticluate systems compared to bare drugs. In addition, the microvasculature pressure in tumors is also one to two times higher than in normal tissues which could enhance the extravasation of nanoparticulate. Many types of nanoparticluate systems could successfully overcome the IFP barrier and leading to selectively enhanced accumulation in the tumors. [12, 13]

3) pH:

Tumors exhibit a lower extracellular pH than normal tissues, as compared to intracellular pH of cells which is similar in both healthy and tumor tissues. The average extracellular tumor pH is between 6.0 and 7.0 (could vary based on the tumor region) while in normal tissues and blood, the extracellular pH of is around 7.4. Low pH and low pO_2 have significant role in the progression of tumor from in situ to invasive cancer. The low extracellular tumor pH could be resulted from the high glycolysis rate in hypoxic cancer cells. However, tumor cells use the same ATP-generating pathway when oxygen is available. Thus, tumor cells do not incorporate the full capacity of glucose oxidation to produce energy (Warburg effect), which is due to defects in the mitochondrial respiratory chain and the need of glycolysis-derived biosynthetic intermediates. Pyruvate is converted into lactate to generate nicotinamide adenine NAD+, a factor required by different glycolytic enzymes in order to maintain a high glycolytic rate. However, lactate itself needs to be eliminated from the cell contributing to metabolic flux and avoid cytotoxicity development. Mono-carboxylate transporter could export one proton along with one lactate molecule, resulting in a progressive acidification of the tumor extracellular space (as well as slight alkalization of the cytosol). Hypoxia could induce the

expression of carbonic anhydrase IX (CA IX) which leads to exacerbate the pH gradient between the intra- and extracellular compartments. This could be caused by conversion of CO_2 to bicarbonate followed by the uptake of this weak base through the anion exchanger Cl-/bicarbonate. Therefore, the resulting pH gradients could be potential sources of differential drug partitioning and distribution. For instance, in a low pH extracellular environment, the uncharged fraction of a weak acid increases and such a drug can thus more easily diffuse through the cell membrane. The relatively basic intracellular compartment could cause the ionization of the molecule, and therefore enhancing the cytosolic accumulation of the drug. Any additional changes in this process may lead to multi drug resistance (MDR) which is caused by a great number of drug exposures leading to the selection of tumor-cell clones with very acidic organelles that could trap drugs followed by reducing their activity. If this organelle is part of the secretory pathway then the drug will be transported out of the cell by exocytosis and thereby, could not treat the diseased area. [12]

1.2.1 Passive Targeting

Passive targeting is based on the unique properties of the tumor microenvironment which was discussed in detail in previous section. There are two major reasons for passive targeting:

(i) Leaky tumor vasculature, which is highly permeable to macromolecules as compared to normal tissue

(ii) Dysfunctional lymphatic drainage system, which results in enhanced fluid retention in the tumor interstitial space. [14, 15]

Passive targeting is based on the transport of nanoparticulate system through leaky tumor capillary fenestrations into the tumor interstitium and cells by either convection or passive diffusion. Convection is the main transport mode for most large

molecules across large pores when the net filtration rate is zero. However, low-molecular weight compounds, such as oxygen, are mostly transported by diffusion, across the cell membrane, according to a gradient of concentration in which no cellular energy is needed. However, due to interstitial hypertension, the convection through the tumor interstitium is poor, which makes diffusion as the major mode of drug transport. The EPR effect could cause selective accumulation of nanocarriers and drug and has been a promising standard in cancer-targeting drug designing. EPR effect can be observed in almost all human cancers with the exception of hypovascular tumors such as prostate cancer or pancreatic cancer. The EPR effect will be more effective if the nanoparticulate system can evade immune system and circulate for a long period. Thus, at least three properties of nanoparticles should be considered.

(i) The ideal nanoparticluate system size should be in the range of 10 to 100 nm. For efficient extravasation from the fenestrations in leaky vasculature, the size should be much less than 400 nm. In addition, to avoid the filtration by the kidneys, it should be larger than 10 nm whereas to avoid the specific capture by the liver, nanoparticles need to be smaller than 100 nm.

(ii) The charge of the particles should be neutral or anionic to inhibit the renal elimination.

The nanoparticulate system must be hidden from the reticuloendothelial system (RES), which destroys any foreign material through opsonization followed by phagocytosis.

However, there are some disadvantages demonstrated for passive targeting

(i) The passive targeting depends on the degree of tumor vascularization and angiogenesis. Thus extravasation of nanoparticulate systems could change by using different tumor types and anatomical sites.

(ii) The high interstitial fluid pressure of solid tumors prevents adequate uptake and homogenous distribution of drugs in the tumor.

The high interstitial fluid pressure of tumors in regards with the poor lymphatic drainage could explain the size relationship with the EPR effect: the larger and longer-circulating a nanoparticulate system (100 nm) is the more nanoparticles could be retained in the tumor. In addition, smaller molecules readily diffuse. [12, 13, 14, 15]

1.2.2 Active Targeting

In active targeting, targeting ligands are conjugated at the surface of the nanoparticles in order to bind appropriate receptors expressed at the target site. The ligand is chosen in the way it could bind to a receptor overexpressed by tumor cells or tumor vasculature but not expressed by normal cells. In addition, targeted receptors should be expressed homogeneously on all targeted cells. Targeting ligands have two general categories: monoclonal antibodies (mAbs) and antibody fragments and nonantibody ligands (i.e. peptidic).The binding affinity of the ligands influences the tumor penetration because of the “binding-site barrier.” For targets in which cells are easily available (tumor vasculature), due to the dynamic flow environment of the bloodstream, high affinity binding are much more preferred. Ligand targeted therapeutics, are divided into different classes based on their application in drug delivery field. [6, 11, 12, 14]

As compared to passive targeting, active targeting is achieved by delivering nanoparticulate systems to uniquely identified sites while having minimal undesired effect on other tissues. [13, 14]

Active tumor targeting is typically achieved by both local and systemic administration of nanoparticulate systems. By using local drug delivery approach, the cytotoxic drug encapsulated in the nanoparticles could be delivered directly to cancer cells leading to minimum harmful toxicity to neighboring healthy tissues. However, this

method is only useful for primary tumors that have not yet metastasized. For metastatic cancers, the location, abundance and size of tumor metastasis within the body limits its visualization or availability, thereby systematic administration could come into the play for successful treatment. [13, 14] Figure 1-4 is the schematic representation of passive and active targeting mechanism.

In the active targeting strategy, two cellular targets can be distinguished which is discussed in the following section:

(i) The targeting of cancer cell

(ii) The targeting of tumoral endothelium

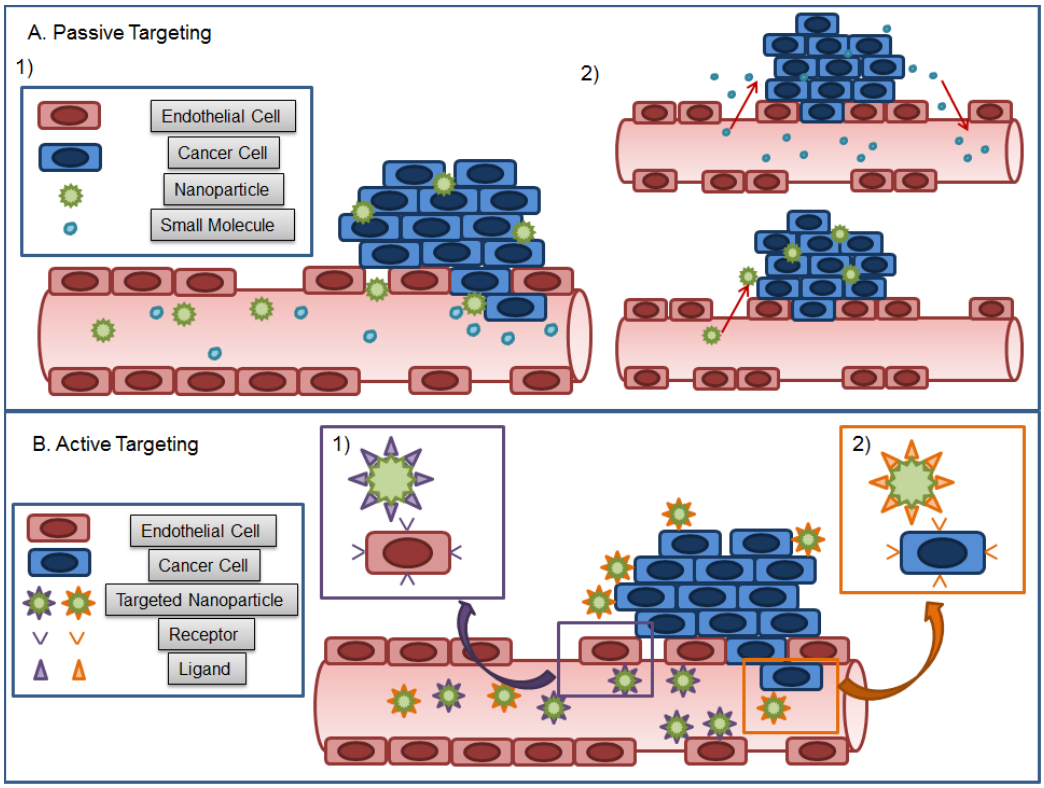

Figure 1-4 A. Passive targeting of nanoparticulate systems: 1) Nanoparticles could reach cancer cells selectively through the leaky vasculature surrounding the tumors. 2) The influence of the size for retention in the tumor tissue. Drugs alone and also other small molecules could diffuse freely in and out the tumor blood vessels because of their small size; thereby their effective concentrations in the tumor decrease rapidly. However, nanoparticulate systems could not diffuse back into the blood stream because of their large size, resulting in progressive accumulation (EPR effect). B. Active targeting of nanoparticulate systems. Ligands conjugated at the surface of nanoparticulate systems could easily bind to receptors (over)expressed by 1) cancer cells or 2) angiogenic endothelial cells. [12]

1.2.2.1 The Targeting of Cancer Cell

The main purpose of active targeting via receptor-mediated internalization is to improve the cellular uptake of the nanoparticulate system. The mechanism is mainly based on intercellular delivery and enhanced cellular internalization rather than an increased tumor accumulation which was the basic for passive targeting. Thus, the ability of the nanoparticles to be internalized after binding to target cell is an important factor in the selection of appropriate targeting ligands. In this strategy, ligand targeted nanoparticulate system could result in direct cell killing, including cytotoxicity against cells that are at the tumor periphery rather than on the tumor vasculature. The more studied receptors for cellular internalization are: Transferrin receptor, Folate receptor, Glycoproteins and Epidermal growth factor receptor. [12]

1.2.2.2 The Targeting of Tumoral Endothelium

Destruction of the endothelium in solid tumors could lead to the death of tumor cells caused by the lack of oxygen and nutrients. The design of nanoparticulate systems which are actively targeted to tumor endothelial cells is based on Judah Folkman suggestion in 1971, demonstrating the idea that the tumor growth might be inhibited by preventing tumors from recruiting new blood vessels. Therefore, in this strategy, ligand-targeted nanoparticulate system could bind to and directly kill angiogenic blood vessels. On the other hand it could indirectly kill the tumor cells that these vessels support, mainly in the tumor core. [12]

The advantages of the tumoral endothelium targeting include:

i) No need of extravasation of nanoparticles to arrive to their targeted site

ii) Possible direct binding to the receptors after intravenous injection

iii) Decreased potential risk of emerging resistance because of the genetically stability of endothelial cells as compared to tumor cells

iv) Expression of most of the endothelial cells markers which is independent of the tumor type, resulting in broad application spectrum

The main targets of the tumoral endothelium include: The vascular endothelial growth factors (VEGF) and their receptors, VEGFR-1 and VEGFR-2, $\alpha_v\beta_3$ integrin, Vascular cell adhesion molecule-1 (VCAM-1), the matrix metalloproteinases (MMPs). [12]

1.2.3 Targeting Molecules for the Development of Targeted Nanoparticles

1.2.3.1 Monoclonal Antibodies

Recently, several antibody-based targeting molecules have been used for their potential application in cancer therapy. Among all, Monoclonal antibodies (mAb) were the firstly introduced ones, and are still the preferred class of targeting molecules. Current studies have been focused on chimeric, humanized, and fully humanized derivatives to reduce their immunogenicity. Some of the clinically used antibody-based drugs include rituximab (Rituxan®), trastuzumab (Herceptin®), cetuximab (Erbitux®), and bevacizumab (Avastin®). Rituximab was FDA approved for treating B-cell lymphoma in 1997. Trastuzumab, which binds to HER2 receptors and was FDA approved for treating breast cancer in 1998. Cetuximab, which binds to epidermal growth factor receptors (EGFR), was approved for treating colorectal cancer in 2004 and head/neck cancer in 2006. Bevacizumab, a tumor angiogenesis inhibitor that binds to vascular endothelial growth factor (VEGF), was approved for treating colorectal cancer in 2004. Even though the previous results have shown significant improvement using mono-therapeutical mAbs, there have been still a number of patients who do not respond to the initial treatment, or exhibit relapses over time. Thus, adjuvant therapies have been introduced, using Abs in combination with chemotherapeutic agents joined by reversible cross-linker. Consequently, each antibody can deliver less than ten drug molecules. To overcome this problem, nanoparticulate systems conjugated with mAbs have been introduced in order

to increase the chemotherapeutic drug loading capacity and to provide some protection to these drugs from metabolism or early excretion. For instance, trastuzumab and rituximab have been conjugated to poly(lactic acid) (PLA) nanoparticles which could increase the rate of particle uptake compared with similar particles without mAb targeting molecules. Even though these systems introduced many advantages, there are still some challenges and limitations that might interfere with getting promising results.

1) mAbs molecules are very large and complex, thereby require significant engineering at the molecular level to be more effective.
2) Antibodies can be expensive especially when manufacturing relative to small-molecule drugs are desired.
3) Antibodies have a hydrodynamic size of ~20 nm that can increase the size of the nanoparticles by up to 40 nm in proportion to the number of antibodies functionalized on them joined onto mAbs using a reversible cross-linker. Consequently, each antibody can deliver less than ten drug molecules which is not adequate for efficient therapy. [12, 14]

1.2.3.2 Aptamer Targeting Molecules

Recently, a novel class of biomolecules, called nucleic acid ligands (aptamers), has been developed for therapeutic and diagnostic applications. Aptamers are DNA or RNA oligonucleotides or modified DNA or RNA oligonucleotides that could be folded by intramolecular interaction into unique conformations with ligand-binding characteristics. Similar to antibodies, aptamers could bind target antigens with high specificity and affinity. There are many advantages reported for aptamers as compared to antibodies. Firstly, aptamers with high affinity for a target can be prepared through in vitro selection and amplification which is called systemic evolution of ligands by exponential enrichment (SELEX). Aptamers isolated using the SELEX process are small (~15 kD as compared

with ~150 kD for antibodies), lack immunogenicity, and could have better tumor/plasma distribution and tumor-penetration properties in comparison with antibodies. Secondly, since the SELEX is a chemical process (no animals used), these ligands can be prepared to bind to any target without considering the toxicity or immunogenicity of the target. Finally, these ligands could be synthesized through chemical oligonucleotide synthesis, which has been shown to scale-up well, with relatively batch to batch consistency in binding affinity as compared to antibodies. [12, 14]

In the last few years, aptamers have attracted much attention as a promising class of biomolecules with variety applications in many areas of science and medicine and more than 200 aptamers have been isolated. The vascular endothelial growth factor (VEGF165) aptamers could lead to regression of tumor vessels as well as exhibiting a remarkable stability in plasma in monkeys. Macugen (Pegaptanib sodium), targeted against the VEGF165, was approved by the FDA in 2004 for the treatment of neovascular macular degeneration. Moreover, conjugation of aptamers to nanoparticles has been widely studied and showed promising results in efficient targeted therapeutics or selective diagnostics as compared to non-targeted nanoparticles. For instance, nanoparticle-aptamer (NP-Apt) conjugates that target the prostate specific membrane antigen (PSMA), a transmembrane protein that is upregulated in a variety of cancers, using the A10 aptamer, was studied. By suing an in vivo tumor model LNCaP prostate cancer cells, which express PSMA antigens, the tumor size had been effectively reduced. [14]

1.2.3.3 Oligopeptide-Based Targeting Molecules

Peptides have been widely used because of their promising properties as targeting ligands. Short peptides (10-15 amino acids) that are able to bind to targeted proteins, cells, or tissues specifically are the most common peptides used in the recent years. Peptides have promising properties as compared to antibodies because of their

small size, lower immunogenicity, higher stability, and ease of manufacture. For instance, Cilengitide® is a cyclic arginine-glycine-aspartic acid (RGD) peptide that binds to integrins and is clinically used for lung and pancreatic cancer. However, RGD-targeted therapy still has some limitations because of nonspecific adhesive nature of the RGD-integrin targeting system. Integrins are extracellular receptors that are both expressed on cancer cells and on all epithelial cells which makes them less specific for cancer. To overcome this problem, recent development of phage display screening methods could successfully isolate peptide ligands with high specificity and affinity to cell-surface hormone receptors (LHRH receptors, somatostatin receptors) and tumor vasculature antigens. [14] Also R11 oligo-arginine peptide has been extensively used because of its prostate cancer specificity, which can be used as a prostate cancer imaging probe. It was shown that, laminin receptor is one of the initial binding sites responsible for R11 peptide uptake in prostate cells. The uptake of R11 is mediated through macropinocytosis [6, 16]

1.2.3.4 Folate-Based Targeting Molecules

One of the most common and widely studied small molecule targeting moieties for drug delivery is folic acid (folate) because folate receptors (FRs) are frequently over-expressed in a range of tumor cells. Folate specifically binds to FRs with a high affinity (KD = ~10^{-9} M), which could deliver and target nanoparticulate system to cancer cells without causing harm to normal cells. Folic acid has been conjugated to many nanoparticulate systems, including liposomes, protein toxins, polymeric NPs, linear polymers, and dendrimers to deliver drugs selectively into cancer cells using FR-mediated endocytosis followed by effective tumor diagnosis and therapy. [12, 14]

However, FRs are expressed both on tumor tissue as well as normal epithelia in the choroids plexus, placenta, lung, intestine, and kidney. Thus, increasing tumor selectivity could be considered for further studies. [14]

1.2.3.5 Other Emerging Targeting Molecules

As discussed in previous sections, mAbs have been caused many challenges and limitations. However, there is still increasing interest in using antibody fragments to improve tumor penetration and meanwhile retaining high antigen binding specificity. [12, 14]

i) Affibody molecules are small polypeptides which are derived from an antibody binding domain of staphylococcal protein. A 6 kD affibody molecule has been reported and widely used with selective binding to HER2 receptor with subnanomolar affinity.

ii) Nanobodies are the smallest fully functional antigen-binding fragment evolved from the variable domain of heavy-chain antibodies. Nanobodies are also low molecular weight <15 kDa polypeptides that show similar antigen binding affinity as affibodies. These small molecules have been shown to improve tumor penetration and lower immunogenicity, since they are a fragment of parent antibody. Recently, a 15 kDa nanobody showed specific uptake in vitro and in vivo.

iii) A-domain proteins are 40-amino-acid oligopeptides that bind to the cell surface through multiple points of attachment. The first A-domain protein introduced was low-density lipoprotein receptor (LDLR).

iv) Avimer is a new class of targeting molecules with a single protein chain containing multiple domains and each of them represents a separate function. Recently, an avimer that binds to interleukin-6 has been used which exhibited higher affinity and specificity compared with A-domain proteins.

v) AdNectins are another class of targeting molecules and are thermostable and protease-resistant oligopeptides which were initially derived from the 10FN3 domain of human fibronectin and each one of them usually has three distinct loop structures. Recently, an AdNectin for human vascular endothelial growth factor receptor 2 (VEGFR2)

named Angiocept used to treat advanced solid tumors and non-Hodgkin's lymphoma in 2006. [14]

Thus, this section summarized different strategies in tumor targeting and consequently conjugation of these biomolecules on nanoparticulate systems may further improve targeted diagnosis and therapy which could be the main goal of this research as discussed in the following.

1.3 Research Project Objectives

1.3.1 Targeting as a Tool to Improve Cancer Diagnosis and Therapy

Recently, mapping and profiling of specific tumor biomarkers characterizing cancer cells were extensively used, followed by understanding of signal cascades involved in the pathogenesis of tumors and consequently, targeted therapies as well as diagnosis in early stage of cancer have become promising topics in cancer research. By designing intelligent new anti-cancer therapeutics improved by targeting biomolecules new avenues in tumor biology have been introduced. The concept of active targeting based on the surface accessibility and the high level of expression of specific cancer antigens, has attracted much attention in the last decade, since it could result in highly efficient treatments and diagnostic modalities, markedly reduced systemic toxicities, as well as offering a unique platform for the design of advanced multifunctional NPs. There are wide range of clinical applications for these nanoparticulate systems in cancer diagnosis and treatment, from specific tumor imaging to targeting conventional chemotherapy, as well as targeting immunotherapy, gene therapy, radiotherapy, photodynamic therapy, phototehrmal therapy and chemoradiation. [14, 16, 17]

By considering the importance of targeted-Nanoparticulate systems which also offer specificity for different kinds of cancer cells, In this study two different nanoparticles synthesized in this lab were used in order to conjugate with variety of biomolecules to

investigate cancer cells targeting which are discussed in detail in the following sections. Figure 1-5 illustrates a summary of the objective of this research.

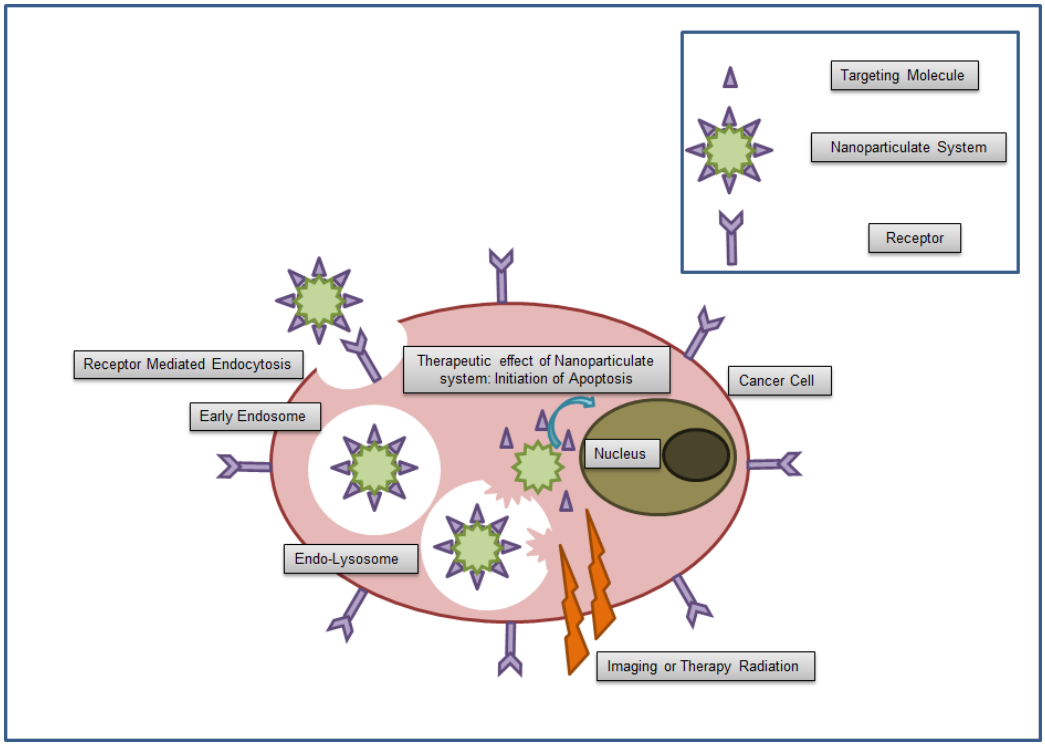

Figure 1-5 Schematic representation of the research project Objectives: Conjugation of biomolecules specific for cancer cells could result in higher cellular internalization followed by enhancement of therapeutic and diagnostic efficiency of cancer cells.

1.3.2 Nanoparticles

1.3.2.1 $Sr_3MgSi_2O_8:Eu^{2+}$, Dy^{3+} Persistent Luminescence Nanoparticles

Firstly, $Sr_3MgSi_2O_8:Eu^{2+}$, Dy^{3+} persistent luminescence nanoparticles (or afterglow NPs) were synthesized in this lab [18, 19, 20]. These nanoparticles maintain luminescence even after the excitation source is removed. Persistent or long afterglow phosphors consist of luminescent materials with long decay lifetimes, ranging from a few minutes to tens of hours. Thus, persistent luminescence could be effectively used in

photodynamic therapy (PDT), since continuing emissions prolong the time that the photosensitizers are activated with the application of additional excitation energy. This could be a promising outcome when radiation is used as the excitation source because radiation doses can be decreased in this manner. [21, 22, 23]

Therefore incorporating luminescent nanoparticles, that combines radiotherapy and photodynamic therapies, has been a novel modality for cancer treatment. In this modality, persistent luminescence nanoparticles conjugated to photosensitizers, such as porphyrins, have been used as a new type of agent for photodynamic therapy. Upon exposure to ionizing radiation such as X-rays, persistent luminescence could be emitted from the nanoparticles and activate the photosensitizers followed by singlet oxygen production resulting in killing of cancer cells. The promising advantage of this approach is that no external light is necessary to activate the photosensitizing agent within tumors. Thus, cancer therapy could be effectively enhanced by combining radiation therapy and PDT as well as reducing the radiation dose. However, one of the most challenging issues is to determine adequate radiation dose to generate enough light for PDT. Tumor necrosis can only occur when the number of absorbed photons exceeds “damage threshold”. In addition, PDT dose is a good parameter for evaluating PDT efficiency, which is the product of the light fluence rate, the molar-extinction coefficient of the photosensitizer, and the photosensitizer concentration in the tumor. One of the common strategies to enhance PDT dose is conjugation of nanoparticulate system with biomolecules, such as folic acid. The afterglow nanoparticles could be excited by irradiation for a few seconds. Then, by ceasing the X-ray source PDT could still be active because of the long afterglow from the selected nanoparticles. This could offer an efficient, simple, convenient, and inexpensive modality for cancer treatment. [22, 23]

Figure 1-6 shows the mechanism of PDT for afterglow nanoparticles, conjugated with photosensitizer.

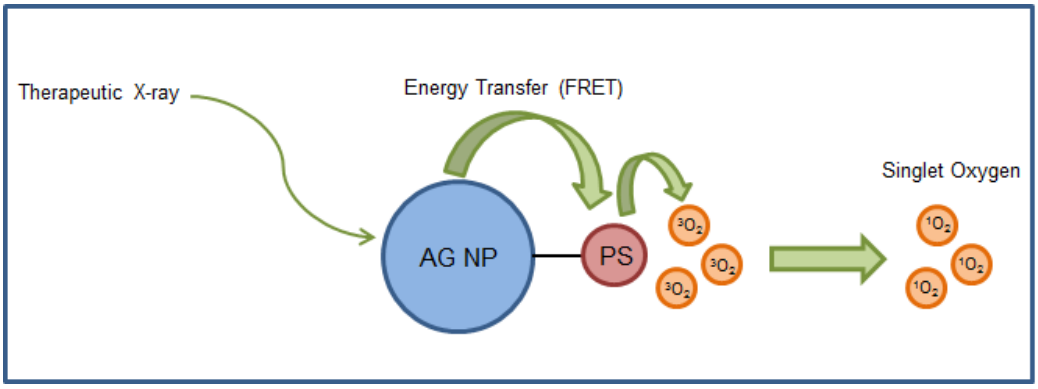

Figure 1-6 Schematic presentation of photodynamic therapy by using persistent luminescence nanoparticles: X-ray could excite the afterglow nanoparticle (AG NP) which transfers the energy to photosensitizer (PS), which reacts with oxygen in the environment and converts it to singlet oxygen. [24]

1.3.2.2 ZnS:Mn Luminescent Nanoparticles

Semi-conductor nanocrystals, which are also called quantum dots (QDs), offer unique optical properties that make them promising candidates as luminescent nanoprobes for biological applications ranging from immunoassays to live cell and tissue imaging. QDs have narrow, symmetrical and tunable emission profiles, high quantum yields, are more robust against photobleaching as compared to conventional dyes and also can be multiplexed by a single excitation source due to their broad absorption profiles, which makes them suitable for long-term imaging. One of the main limitations of using II–VI semiconductor QDs (such as CdSe and CdTe) in biomedical applications is their toxicity because of decomposition and release of heavy metal ions and formation of highly reactive oxygen species. Therefore, recently, non-cadmium-based QDs for

applications in biology gained much more attention. Doped-ZnS QDs are extremely promising and potential candidates since in addition to their cadmium-free structure, they offer stable luminescence and high quantum efficiency. Recently Al^{3+}, Cu^{+}, and Mn^{2+}-multidoped ZnS QDs conjugated to folic acid by have been studied and used for the imaging of cancer cells using confocal microscopy by excitation in a safe spectral range (k > 400 nm). In addition, since the two photon absorption of QDs is much higher than that of organic fluorophores, they can successfully be used for two photon florescent microscopy via excitations from far-red to near infrared wavelengths. [25, 26, 27] Also, three-photon excitation can be used, which occurs when three photons are simultaneously absorbed by nanoparticles through virtual states, resulting in several advantages. This process can be applied to ultraviolet-absorbing luminophores using a NIR pulsed laser, which can prevent the photodamage induced by ultraviolet light, and compete with Rayleigh scattering for imaging thick biological specimens. In addition, the three-photon process should have a higher spatial resolution than two-photon excitation. Although the three-photon process had been used before for auto-fluorescence detection and counterstaining visualization, three-photon biomedical imaging had not been realized because of its intrinsic low quantum mechanical efficiency. In a study by Jung Ho Yu et al. [28] the incorporation of the three-photon excitation of ZnS nanocarriers combined with visible emission from Mn dopants for high-resolution in vitro and in vivo targeted imaging was studied. Therefore, recently, Mn-doped ZnS synthesis has been reported which could be used for confocal, two photon and three photon imaging. [26, 27, 28]

Thus, the second nanoparticle used in this project was ZnS:Mn luminescent nanoparticles which were synthesized in this lab [29] with red emission luminescent properties which make them promising candidates for in vitro and in vivo imaging in cancer diagnosis field.

1.3.3 Conjugation to verity of biomolecules for cancer cells targeting

1.3.3.1 Folic Acid

Folate receptors are the most widely studied receptors, as they are upregulated on a variety of human cancers, including breast, ovaries, endometrium, renal cell carcinoma, lungs, kidneys, colon, brain metastases, colorectal, and neuroendocrine carcinoma due to their enhanced mitosis rates. This over-expression of folate receptors (FR) on cancer tissues which is called tumor biomarkers could be used to target folic acid-conjugated NPs as imaging and therapeutic agents specifically to FR expressing tumors, resulting in less uptake by healthy tissues that express few or no FR. Also, when the stage of cancer advances, the expression of FR increases. The FR is a glycosyl phosphatidylinositol-linked membrane glycoprotein having the apparent molecular weight of 38–40 KDa. Thus, folic acid is a short chain, non-immunogenic and high affinity ligand which is an essential precursor for the synthesis of nucleic acid and some amino acids. It is not endogenously produced by mammalian cells and requires internalization by cells either via receptor-mediated endocytosis or carrier-based uptake mechanism. Studies showed that conjugation of folic acid to anticancer drugs, liposomes, nanoparticles and micelles could enhance their cellular uptake. Moreover, since, FR is expressed on the basolateral surface (blood side) of transformed cells as compared to the apical surface expression in most of the normal cells (i.e. breast tissue), cancer cell specificity of folic acid as a targeting agent when delivered through the blood could be explained. They can also be used for other applications, including immunodetection, bioimaging, folic acid-based biosensors, hyperthermia, and study of the cell signaling mechanism. [30]

In a study by Li-Qin Xiong, et al. [31] they incorporated folic acid-conjugated upconversion nanophosphores which could enhance targeted upconversion luminescent

imaging of FR-overexpressing HeLa tumor (which is folate receptor positive compared to MCF-7 cell lines) in vivo and ex vivo.

In another approach Folic acid-functionlized upconversion luminescent nanoparticles (FA-UCNPs) have been demonstrated to be effective in targeting folate-receptors overexpressing cancer cell lines (KB cell lines) as compared to MCF-7. [32]

In another study by et al. [33] folate-conjugate poly [(p-nitrophenyl acrylate)-co-(N-isopropylacrylamide)] submicrogels (F-SubMGs) as 5-Fluorouracil (5-FU) delivery systems were introduced. It was shown that the presence of folate in those submicrogels systems could improve their internalization in HeLa cells, which are folate receptor positive. However, it was shown that in the case of MCF-7 line, it is mainly produced by a nonspecific mechanism.

However, in another study it was demonstrated that the 70-nm FA-Se nanoparticles were internalized by MCF-7 cells through folate receptor-mediated endocytosis and targeted to mitochondria through endocytic vesicles transporting followed by entering into mitochondria and as well as triggering the mitochondria dependent apoptosis of MCF-7 cells (oxidative stress, Ca^{2+} stress changes, and mitochondrial dysfunction and damaging). FA-Se nanoparticles could be released from broken mitochondria and transported into nucleus and induced MCF-7 cell cycle arrest. In addition, FA-Se nanoparticles could induce cytoskeleton disorganization as well as MCF-7 cell membrane morphology changes. [34]

In one study, it was shown that the FA-lipid-based nanoparticles could deliver genes extensively to FR-negative LNCaP and PC-3 cells, as well as FR positive KB and Hela cells. [35]

Other studies also showed that under same conditions, cytotoxicity of QDs in the folic acid conjugated poly (lactide)-vitamin E TPGS (PLA-TPGS) and vitamin E TPGS-

carboxyl (TPGS-COOH) nanoparticles were demonstrated and was lower for normal cells such as NIH 3T3 cells than that for breast cancer cells such as MCF-7 (folate receptor positive compared to NIH 3T3 cells) due to folate targeting effect. [36]

Also Retnakumari, Archana, et al. [37] showed that the emission intensity of gold-bovine serum albumin- folic acid (Au–BSA–FA) nanocarriers at 674 nm was higher for KB cell lines in comparison with MCF-7 cell lines but lower for A549 cell lines as compared to MCF-7 cell lines. This, Au–BSA–FA conjugates were taken up by KB and MCF-7 cells through FR-mediated endocytosis and the relative changes in the uptake is due to different expression levels of the receptor in those cell lines.

Finally, in another study, the same cell lines were used for dual targeting of folate-conjugated hyaluronic acid polymeric micelles for paclitaxel delivery. [38]

Thus, in this project afterglow nanoparticles were conjugated to folic acid through a simple EDC/NHS (1-Ethyl-3-(3-dimethylaminopropyl) carbodiimide /N-hydroxysuccinimide) chemistry. Then, some characterization studies were performed. The luminescence properties of NPs after conjugation were studied. UV-vis absorption spectra was used to confirm conjugation, as well as calculating the conjugation efficiency. Zeta potential was performed using dynamic light scattering (DLS) device to confirm the FA conjugation to NPs. The size of NPs after conjugation was measured using DLS. Cell viability studies were done using MTT assay. Finally fluorescent imaging was done using PC-3 cells (negative for folic acid) MCF-7 (positive for folic acid compared to PC-3 cells) and KB cells (positive for folic acid) to compare the cellular uptake and confirm targeted delivery. These persistent luminescence nanoparticles could be further conjugated with photosensitizer so they can be used for targeted photodynamic therapy especially for breast cancer cells, since our lab have been focused more on breast and prostate cancer cells targeting which are one of the most common cancers and the second cause of

death among women and men, respectively, according to cancer statistics 2012. [39] Figure 1-7 illustrates the mechanism by which the afterglow nanoparticles conjugated to photosensitizer and targeting moiety (folic acid) could be specifically uptaken by cancer cells which over-expressed folate receptors (receptor mediated endocytosis). Consequently the nanoparticulate system, could enter early endosome, followed by endo-lysosome and finally will be released toward the mitochondria by irradiation of X-ray. This irradiation could excite the afterglow nanoparticles and cause the energy transfer from these nanoparticles to photosensitizer which could produce singlet oxygen species resulting in cancer cell death.

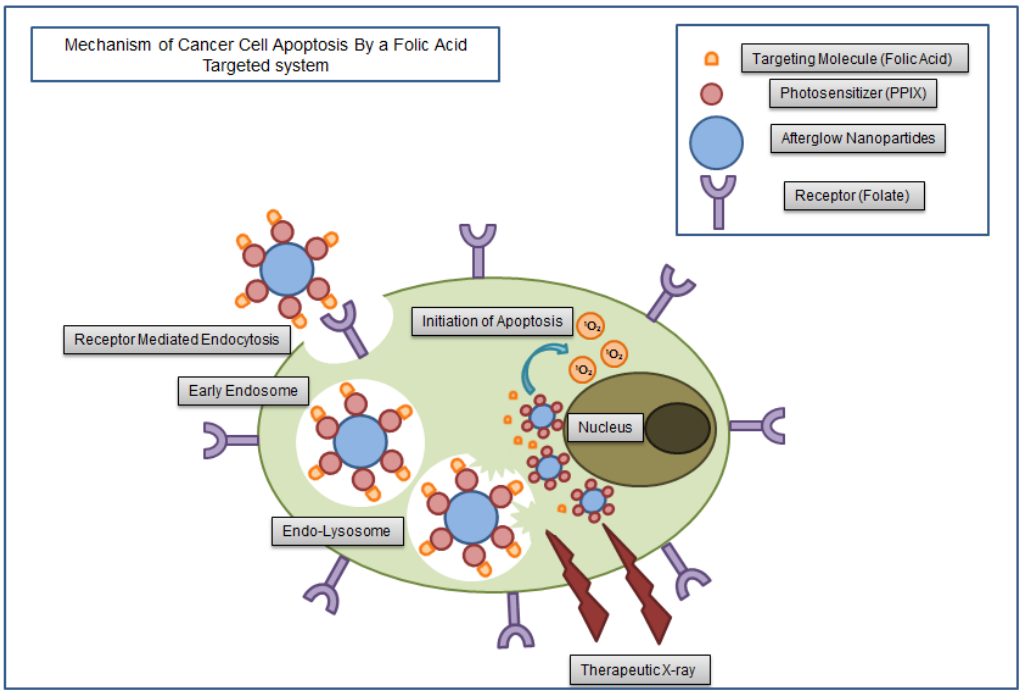

Figure 1-7 Schematic representation of receptor-mediated endocytosis of folic acid-conjugated afterglow nanoparticle-photosensitizer system in cancer cells followed by cancer cell apoptosis. [30]

1.3.3.2 RGD Peptide

'Homing' peptides are promising modalities for tumor targeting because they bind to surface molecules specific to the tumor, and tumor endothelial and tumor lymphatic cells, but are smaller than other agents such as antibody fragments, which allow them to easily penetrate tumor tissues. One of the most studied example for homing peptides is an Arg-Gly-Asp (RGD) which is present in many extracellular matrix components such as fibronectin and vitronectin, and could target RGD-peptide receptor, α(v) integrins, in tumor blood vessels and on the surface of tumor cells. Peptides containing the RGD sequence are commonly used in targeted tumor imaging and therapy through coupling with therapeutic agents such as radionucleotides and chemotherapeutic drugs. RGD peptide could bind tumor endothelial cells as well as tumor cells in vitro and vivo, followed by tumor internalization of RGD peptide. It is known that α(v) integrins can enhance and mediate adhesion and migration in some tumor cell lines and regulate cell proliferation and survival. [40] Among the known 24 integrin subtypes, integrin $\alpha_v\beta_3$ has been widely studied for tumor imaging and therapy because of its important roles in angiogenesis, growth, and metastasis of some tumors. Recently, integrin $\alpha_v\beta_3$ has attracted much attention in diagnostic imaging of tumor angiogenesis because of its high expression on activated and proliferating endothelial cells during tumor angiogenesis and metastasis as comparison with resting endothelial cells and most normal organs. Thus, diverse RGD peptide ligands have been introduced to target integrin $\alpha_v\beta_3$ and angiogenic vessels. Among all, a class of cyclic RGD penta-peptide analogs including c(RGDfV) and c(RGDfK) is a promising candidate due to its high receptor binding affinity and specificity. [41, 42]

QD705-RGD conjugated to 2 μM c(RGDyK) showed strong binding and fluorescence signal when using integrin-positive MDA-MB-435 and U87MG cells as

compared to integrin $\alpha_v\beta_3$ -negative MCF-7 cells (human breast cancer cell line). In addition, [41, 43]

In a report by Zhe Wang et al. [42] it was shown that the most significant uptake of multifunctional PLGA nanoparticles was observed at 4 h incubation in B16F10, DU145 and MDA-MB-23 cells which are positive for integrin $\alpha_v\beta_3$. Because MCF-7 cell lines lack the integrin $\alpha_v\beta_3$ on their cell membrane [43] the uptake of cRGD modified nanoparticles into these cells was few over the 4-h incubation period. However, there was little nonspecific association to cells after 4 h.

Herein, the persistent luminescence nanoparticles were used to conjugate cyclic RGDfK peptide with two different methods. Then fluorescent imaging was done using MDA-MB-231 breast cancer cell line as positive for $\alpha_v\beta_3$ integrin receptor and MCF-7 as negative for $\alpha_v\beta_3$ integrin receptor to compare the cellular uptake and confirm targeted delivery.

The main reason that we chose RGD peptide over folic acid was the more specificity of RGD peptide to breast cancer cells as compared to folic acid which receptor is overexpressed in variety of cancers. [30, 44] Also there are many advantages for RGD peptide compared to other ligands:

i) RGD is much smaller as compared to monoclonal antibodies, thereby RGD conjugates can have easier access to the tumor tissue

ii) The use of RGD minimizes immune reactivity or pathogen transfer risk

iii) The synthesis of RGD peptides is relatively simple and inexpensive, so it can easily be used in clinical applications

iv) There are much wider applications for RGD as compared to folic acid, since it can be used in tumor therapy as well as coupling with material surfaces in controlled densities and orientations. [45]

1.3.3.3 PSMA Inhibitor

Prostate cancer is the second leading cause of death among men in united states [39] One of the strategies to treat prostate and other types of cancer involves tumor antigens specific targeting. Identification of several prostate antigens could lead to introducing several possible candidates for targeted diagnosis and therapy. The most common antigen is the prostate specific membrane antigen (PSMA). PSMA is a type II membrane protein with folate hydrolase activity and is over-expressed in prostate cancer, its metastatic form, and the hormone-refractory form and the neovasculature of many non-prostate solid tumors. [46, 47, 48, 49]

In one study it was demonstrated that the uptake of PSMA conjugated QDs with LNCaP prostate cancer cells (a PSMA-positive cell line) was more significant as compared to unconjugated QDs. Also, in this in vitro study, there was no detectable uptake of PSMA conjugated QDs by PC-3 cells (a PSMA-negative cell line). [50, 51]

It was also shown that the aptamer-facilitated cellular uptake of the Pt (IV)-encapsulated nanoparticles by PSMA positive LNCaP cells via endocytosis was higher as compared to PC-3 cells which are negative for PSMA inhibitor. [47]

Other reports also demonstrated the same results for LNCaP and PC-3 cellular uptake by using different nanoparticulate devices, such as docetaxel-encapsulated, pegylated PLGA NPs-Apt bioconjugates [48] pegylated PLA nanoparticles and microparticles as a microfluidic model [52] and rhodamine-labeled dextran (as a model drug) and developed drug encapsulated pegylated PLA nanoparticles with a negative surface charge. [53]

Herein, the ZnS:Mn luminescent nanoparticles were used to conjugate to phosphonic acid-based NAALADase inhibitors. NAALADase is expressed in the human prostate parenchyma, from where it was first cloned and named prostate specific

membrane antigen (PSMA). It has been shown that inhibitors of NAALADase also strongly bind to PSMA. [54]

In addition, LNCaP and PC-3 cell lines were used as positive and negative for PSMA receptors followed by in vitro fluorescent imaging to compare the cellular uptake and confirm targeted delivery.

1.3.3.4 R11 Peptide

Receptor-mediated targeting has been widely used by incorporating targeting ligands (i.e. RGD and folic acid) to target the prostate cancer. However, these targeting ligands can find their targets in other cancer types as well so they could not offer tumor specificity. One strategy to increase the specificity of biological targets is to use a cancer-specific ligand, such as cell-penetrating peptides (CPPs). CPPs are capable of crossing cell membrane via macropinocytosis mechanism which could deliver CPPs to the intracellular systems. Among all of the CPPs, arginine-rich CPPs including HIV-Tat peptides and oligoarginines have been studied and showed high internalization efficacy. Novel researches tried to use polyarginine peptide (R11) which has prostate cancer specificity as a cancer imaging probe. [6, 16]

In one study, R11-conjugated PNIPAAm-AAm-AH-coated magnetic nanoparticles (R11-PMNPs) could efficiently target prostate cancer and monitor tumor response to treatment using non-invasive imaging modalities. Also, higher nanoparticle uptake was observed by LNCaP cells compared with those of PC3 cells. [6] In addition, significantly higher uptake of PLGA nanoparticles conjugated with R11 by PC-3 cells than the PLGA nanoparticles conjugated with other targeting ligands such as RGD and folic acid was also studied. Thus, the results demonstrated that the R11 peptides show greater specificity toward prostate cancer cells as compared to other CPPs. [6]

Also, R11 seemed to be the best efficient delivery system among the peptides tested in several prostate cancer cell lines. The uptake could be detected within 5 minutes in prostate cancer cells right after exposure to CPP. [55]

Herein, the persistent luminescence nanoparticles were conjugated to R11-SH peptide provided by Dr.Jer-Tsong Hsieh's lab at UT Southwestern Medical Center at Dallas [16]. Fluorescent Imaging was performed on LNCaP and PC-3 cells as models for prostate cancer cell lines and the uptake was studied.

Chapter 2

Materials and Methods

2.1 Folic acid Conjugation to persistence luminescence nanoparticles

2.1.1 Materials

Folic acid (FA), 1-Ethyl-3-(3-dimethylaminopropyl)carbodiimide (EDC), N-hydroxysuccinimide (NHS), (3-Aminopropyl) triethoxysilane (APTES), fetal bovine serum (FBS; 10%), Penicillin/Streptomycin, paraformaldehyde (PFA), Sodium hydroxide (NaOH), sterilized phosphate buffered saline (PBS), and Trypsin were all purchased form Sigma-Aldrich. MTT reagent was purchased from Trevigen Inc. $Sr_3MgSi_2O_8:Eu^{2+}$, Dy^{3+} persistent luminescence nanoparticles were synthesized in this lab [20]. KB cells (ATCC number CCL-17), MCF-7 cells (ATCC number HTB-22), PC-3 cells (ATCC number CRL-1435), Eagle's minimum essential medium (EMEM) and F-12 K medium were all purchased from ATCC company. VECTASHIELD® Mounting Medium with PI was purchased from Vector Company. Toluene (mallinckrodt Chemicals Company) and Dimethyl sulfoxide (DMSO) (VWR International) were used as solvents.

2.1.2 Methods

2.1.2.1 Wet Grinding Method for Reducing the Size of Persistent Luminescence Nanoparticles (NaOH Soaking)

Nanometer-sized particles of $Sr_3MgSi_2O_8:Eu^{2+}$, Dy^{3+} obtained by basic wet grinding of the solid for 20 minutes with a mortar and pestle in a minimum volume of 10 mM NaOH solution (~ 200 µl). Furthermore, hydroxylation was performed overnight by dispersing the ground powder in 20 mL of the same NaOH solution to get hydroxyl-afterglow nanoparticles. [20, 56]

2.1.2.2 APTES Coating on Persistent Luminescence Nanoparticles

The synthesized afterglow nanoparticles (AG NPs) were coated with APTES to introduce NH_2 groups on the surface of the nanoparticles which already had OH functional groups on their surface. The silanol groups present on the external surface of the nanoparticles react with the Aminopropyltryethoxy Silane (APTES) through formation of Si-O-Si bridges. The introduced amine groups on their external surface were then further conjugated with folic acid. [57, 58]

To this end, 1ml APTES was added to the solution of 10 mg nanoparticles in 25 ml toluene which was previously sonicated well. Then the mixture was heated up to (80-110°C) under constant stirring, reflux and N_2 gas to provide ambient environment for silanization reaction. Then the reaction was kept overnight to ensure functionalization of nanoparticle followed by centrifugation and washing with toluene and ethanol to remove unreacted reagents and prepare for next conjugation step. [20, 59, 60, 61] Figure 2-1 illustrates the APTES coating reaction on the surface of the AG NPs in toluene at high temperatures.

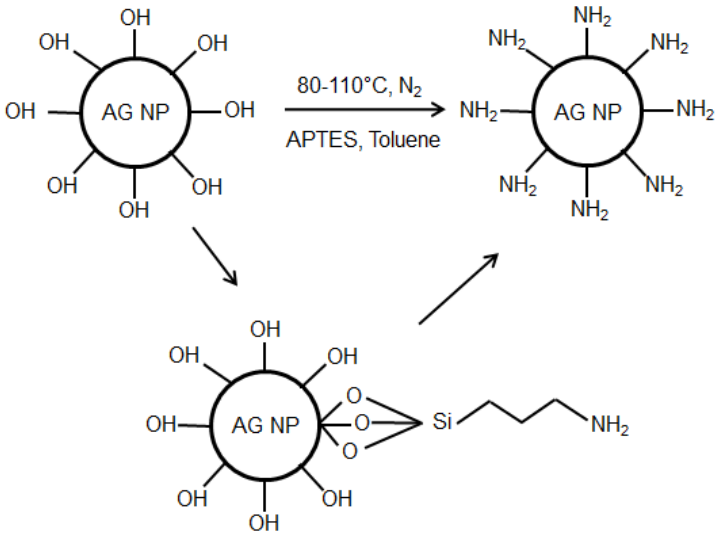

Figure 2-1 Schematic of APTES coating on the surface of AG NPs

2.1.2.3 Conjugation of Folic Acid to Persistent Luminescence Nanoparticles

Folic acid was conjugated to AG NPs using the well-known EDC/NHS chemistry as discussed in previous protocols. All the ratios were chosen based on the efficacy of the results as well as maintaining the afterglow properties of the nanoparticles. [25, 27, 31, 62-65] Briefly, FA (5 mg, 1.13×10^{-5}mol) was dissolved in 1.5 ml DMSO and activated by EDC (13.5 mg, 7×10^{-5}mol) under nitrogen gas and constant stirring at room temperature (RT) and in dark environment for 20 minutes. Then, NHS (8 mg, 7×10^{-5}mol) was added and the reaction was continued for 1 hour at room temperature. The activated FA solution was added dropwise to dissolved AG NPs in 1 ml DI water (10 mg, 2.12×10^{-5} mol), followed by a reaction under constant stirring at RT for 24 hours. Finally, the resulting nanoparticles were centrifuged and washed three times with DMSO, Water and PBS to remove all the unreacted reagents. Figure 2-2 illustrates the procedure of FA conjugation to AG NPs at room temperature using the prepared APTES coated NPs in previous section.

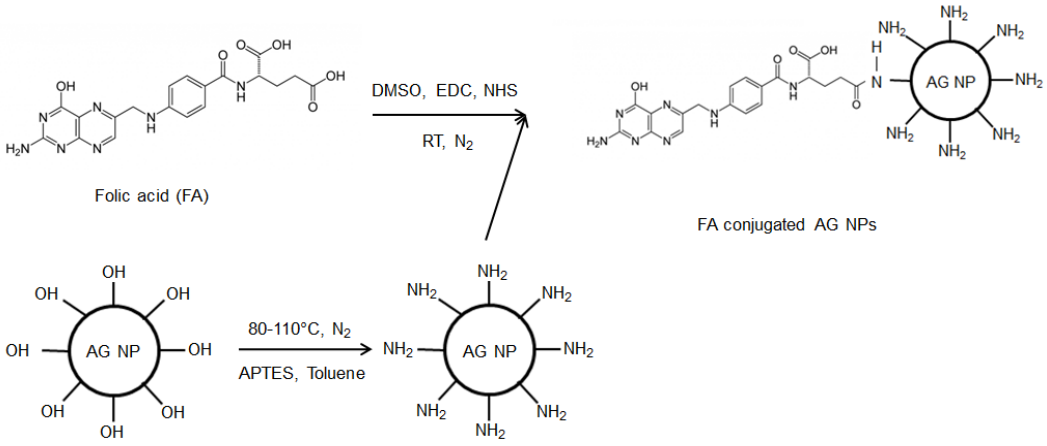

Figure 2-2 Schematic of FA conjugation to AG NPs

2.1.2.4 Florescence Spectrophotometer

The luminescence emission spectra were measured using a Shimadzu RF-5301PC spectrofluorophotometer.

2.1.2.5 UV-Vis Absorption Spectrophotometer

The optical absorption spectra were recorded on a Shimadzu 2450 ultraviolet–visible (UV–VIS) spectrophotometer. This device was used to confirm the FA conjugation as well as calculating the conjugation efficiency. [64]

2.1.2.6 Dynamic Light Scattering (Size and Zeta Potential)

The size of nanoparticles before conjugation, after NaOH soaking and conjugation, after conjugation and filtration was studied using Dynamic Light Scattering (DLS) method (Zeta PALS, Zeta potential analyzer, Brookhaven Instruments).

Also the surface charge of the nanoparticles before conjugation, after NaOH soaking, after APTES coating and after conjugation to FA was studied by using DLS device, in order to study the surface charge and stability of the nanoparticles as well as to confirm FA conjugation to AG NPs. [27]

2.1.2.7 Cell Viability

Human prostate carcinoma cell line PC-3 (ATCC number CRL-1435) was cultured in F-12 K medium supplemented with 10 % fetal bovine serum (FBS) and 1 % penicillin–streptomycin solution followed by seeding in a 96 well plate. The cells were treated with four concentrations of nanoparticles including 500 µg/ml, 250 µg/ml, 125 µg/ml, 62.5 µg/ml and incubated for 24 hours. Then, 10µl of 5 mg/ml MTT solution was added to each well and incubated for 4 h at 37 °C under 5% CO_2. The supernatant was then removed and cells are lysed with 100 µl DMSO. Using a microplate reader, absorbance was recorded at 570nm to determine cell survival. [66, 67]

2.1.2.8 Fluorescent Microscopy

Human nasopharyngeal epidermal carcinoma cell line, KB cells (ATCC number CCL-17), Human epithelial breast cancer cell line (ATCC number HTB-22) were cultured in EMEM and human prostate carcinoma cell line PC-3 (ATCC number CRL-1435) was cultured in F-12 K medium, supplemented with 10% FBS and 1 % penicillin–streptomycin solution at 37°C (5% CO_2). Furthermore, cells were seeded in a 6-well plate and then the cells were treated with 100 µg/ml nanoparticles. Cells were fixed with freshly prepared 4% paraformaldehyde (PFA) for 5 min and then washed three times with PBS. The cell nuclei were then stained with PI for 10 min followed by washing three times with PBS. PI is a reddish nuclear counterstain with a broad excitation range at around 535 nm and emission at about 615 nm when bound to DNA (www.vectorlabs.com). Fluorescence imaging was used (Olympus 1X71 inverted fluorescence microscope) in order to study and compare the cellular uptake for three different cell lines. [66, 67]

2.2 RGD peptide Conjugation to Persistent Luminescence Nanoparticles

2.2.1 Materials

1-Ethyl-3-(3-dimethylaminopropyl)carbodiimide (EDC), N-hydroxysuccinimide (NHS), (3-Aminopropyl) triethoxysilane (APTES), 2-(N-morpholino)ethanesulfonic acid (MES buffer), fetal bovine serum (FBS; 10%), Penicillin/Streptomycin, paraformaldehyde (PFA), sterilized phosphate buffered saline (PBS), Sodium hydroxide (NaOH), and Trypsin were all purchased form Sigma-Aldrich, $Sr_3MgSi_2O_8:Eu^{2+}$, Dy^{3+} persistent luminescence nanoparticles were synthesized in this lab [20], Cyclo (- RGDfK) was purchased from AnaSpec company, MCF-7, MDA-MB-231 cell lines and Dulbecco's Modified Eagle Medium (DMEM) were provided form University of Texas Southwestern Medical Center at Dallas. VECTASHIELD® Mounting Medium with PI was purchased from Vector Company. Eagle's minimum essential medium (EMEM) was purchased from

ATCC company. Toluene (mallinckrodt Chemicals Company) and Dimethyl sulfoxide (DMSO) (VWR International) were used as solvents.

2.2.2 Methods

2.2.2.1 Conjugation of RGD Peptide to Persistent Luminescence Nanoparticles (Method 1)

Firstly, the same method for nanoparticles wet grinding (NaOH soaking) and APTES coating, as discussed earlier for folic acid conjugation, was used to prepare AG NPs with NH_2 on the surface to further conjugate with COOH group on the surface of RGD peptide. To this end, RGD peptide (0.5 mg, 8.28×10^{-4} mmol) was dissolved in 1 ml DMSO. Then EDC (10mg, 6.44×10^{-2} mmol) was added followed by constant stirring at room temperature, under N_2 gas, in dark. After 5 minutes, NHS (10mg, 8.69×10^{-2} mmol) was added. The resulting solution was added dropwise to a solution of AG NPs (10 mg, 2.12×10^{-5} mol) at room temperature under N_2 gas and constant stirring, in dark and the reaction was kept overnight. Subsequently the suspension was centrifuged and washed three times with DMSO, DI water and PBS. [59, 62] Figure 2-3 illustrates the procedure of RGD peptide conjugation to AG NPs using DMSO as a solvent.

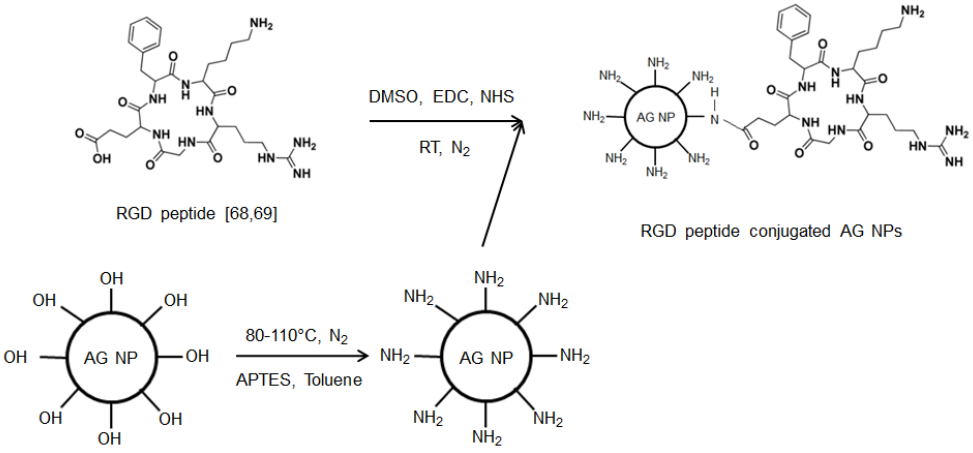

Figure 2-3 Schematic of RGD peptide conjugation to AG NPs

2.2.2.2 Conjugation of RGD Peptide to Persistent Luminescence Nanoparticles (Method 2)

Since, the RGD peptide used in this project had both NH_2 and COOH functional groups, another common method could be used to conjugate the RGD peptide to AG NPs. Plasma coated AG NPs (Plasma coating was done by Professor Timmons' lab, department of Chemistry and Biochemistry, University of Texas at Arlington) were used in order to conjugate to RGD peptide.

Firstly, Plasma coated AG NPs (10 mg, 2.12×10^{-5} mol) were dissolved in 10 ml 0.05 M MES buffer solution (pH=6). Then EDC (10mg, 6.44×10^{-2} mmol) was added followed by constant stirring at room temperature, under N_2 gas, in dark. After 15 minutes, NHS (10mg, 8.69×10^{-2} mmol) was added followed by adding RGD peptide (0.5 mg, 8.28×10^{-4} mmol) at room temperature under N_2 gas and constant stirring, in dark and the reaction was kept overnight. Subsequently the suspension was centrifuged and washed three times DI water and PBS. [70, 71, 72] Figure 2-4 illustrates the procedure of RGD peptide conjugation to plasma coated AG NPs.

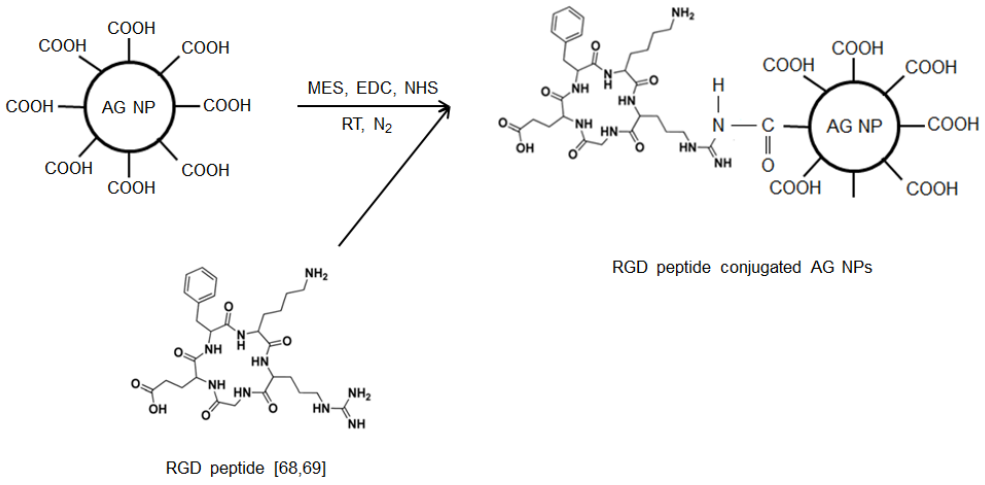

Figure 2-4 Schematic of RGD peptide conjugation to plasma coated AG NPs

2.2.2.3 Fluorescent Microscopy

MCF-7 and MDA-MB-231 cells were cultured in EMEM and DMEM, respectively and supplemented with 10% FBS and 1 % penicillin–streptomycin solution at 37°C (5% CO_2). Furthermore, cells were seeded in a 6-well plate and then the cells were treated with 100 µg/ml nanoparticles. Cells were fixed with freshly prepared 4% paraformaldehyde (PFA) for 5 min and then washed three times with PBS. The cell nuclei were then stained with PI for 10 min followed by washing three times with PBS. PI is a reddish nuclear counterstain with a broad excitation range at around 535 nm and emission at about 615 nm when bound to DNA (www.vectorlabs.com). Fluorescence imaging was used (Olympus 1X71 inverted fluorescence microscope) in order to study and compare the cellular uptake for two different cell lines as well as two different conjugation methods. [66, 67]

2.3 PSMA Inhibitor Conjugation to ZnS:Mn Luminescent Nanoparticles

2.3.1 Materials

1-Ethyl-3-(3-dimethylaminopropyl)carbodiimide (EDC), N-hydroxysuccinimide (NHS), 2-(N-morpholino)ethanesulfonic acid (MES buffer), fetal bovine serum (FBS; 10%), Penicillin/Streptomycin, paraformaldehyde (PFA), sterilized phosphate buffered saline (PBS), and Trypsin were all purchased form Sigma-Aldrich, ZnS:Mn luminescent nanoparticles were synthesized in this lab [29], 2-(Phosphonomethyl)-pentanedioic acid, NAALADase inhibitor (PSMA inhibitor) was purchased from Enzo Life Science company, PC-3 cells (ATCC number CRL-1435) and LNCaP cells (ATCC number CRL-1740), Eagle's minimum essential medium (EMEM) and F-12 K medium were all purchased from ATCC Company. VECTASHIELD® Mounting Medium with DAPI was purchased from Vector Company. Dimethyl sulfoxide (DMSO) (VWR International) was used as a solvent.

2.3.2 Methods

2.3.2.1 Conjugation of PSMA Inhibitor to ZnS:Mn Luminescent Nanoparticles (Method 1)

Since, PSMA inhibitor used in this project had COOH functional groups, three methods were used to conjugate the PSMA inhibitor to ZnS:Mn nanoparticles. ZnS:Mn NPs already had NH_2 groups on the surface which had been introduced during synthesis process. [29]

Firstly, PSMA inhibitor (0.3 mg, 1.33×10^{-3} mmol) was dissolved in 5 ml DI water Then EDC (10mg, 6.44×10^{-2} mmol) was added followed by constant stirring at room temperature, under N_2 gas, in dark. After 15 minutes, NHS (10mg, 8.69×10^{-2} mmol) was added followed by adding ZnS:Mn nanoparticles (5 mg, 5.13×10^{-2} mmol) at room temperature under N_2 gas and constant stirring, in dark and the reaction was kept overnight. Subsequently the suspension was centrifuged and washed three times DI water and PBS. [46, 48, 52]

2.3.2.2 Conjugation of PSMA Inhibitor to ZnS:Mn Luminescent Nanoparticles (Method 2)

Firstly, PSMA inhibitor (0.3 mg, 1.33×10^{-3} mmol) was dissolved in 5 ml PBS buffer solution (10%, pH=7.4). Then EDC (10mg, 6.44×10^{-2} mmol) was added followed by constant stirring at room temperature, under N_2 gas, in dark. After 15 minutes, NHS (10mg, 8.69×10^{-2} mmol) was added followed by adding ZnS:Mn nanoparticles (5 mg, 5.13×10^{-2} mmol) at room temperature under N_2 gas and constant stirring, in dark and the reaction was kept overnight. Subsequently the suspension was centrifuged and washed three times DI water and PBS. [73]

2.3.2.3 Conjugation of PSMA Inhibitor to ZnS:Mn Luminescent Nanoparticles (Method 3)

Firstly, PSMA inhibitor (0.3 mg, 1.33×10^{-3} mmol) was dissolved in 5 ml MES buffer solution (0.05 M, pH=5.5-6). Then EDC (10mg, 6.44×10^{-2} mmol) was added followed by constant stirring at room temperature, under N_2 gas, in dark. After 15

minutes, NHS (10mg, 8.69×10^{-2} mmol) was added followed by adding ZnS:Mn nanoparticles (5 mg, 5.13×10^{-2} mmol) at room temperature under N_2 gas and constant stirring, in dark and the reaction was kept overnight. Subsequently the suspension was centrifuged and washed three times DI water and PBS. [63, 70-72, 74]

Figure 2-5 illustrates the procedure of PSMA inhibitor conjugation to ZnS:Mn NPs using three different solvents.

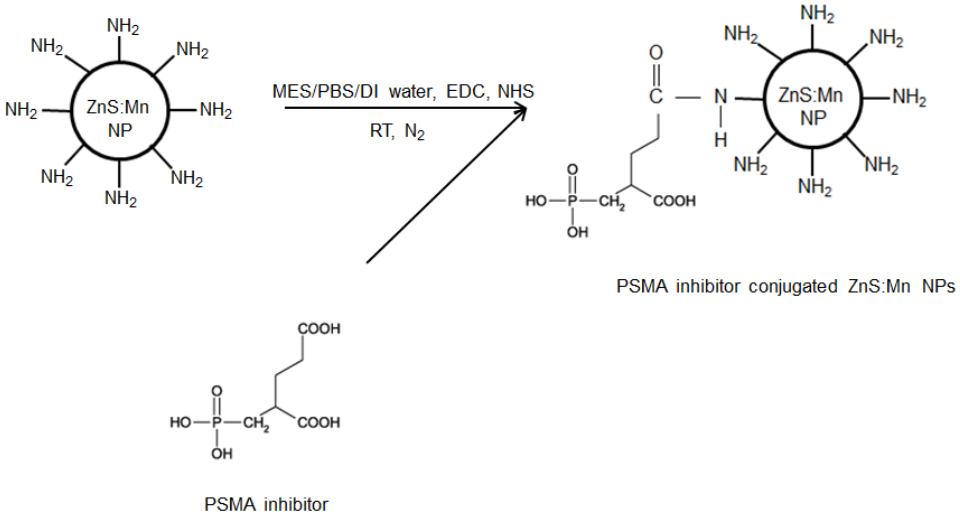

Figure 2-5 Schematic of PSMA inhibitor conjugation to ZnS:Mn NPs using three different solvents (method 1, 2 and 3)

2.3.2.4 Fluorescent Microscopy

PC-3 and LNCaP cells were cultured in F-12 K and EMEM medium, respectively and supplemented with 10% FBS and 1 % penicillin–streptomycin solution at 37°C (5% CO_2). Furthermore, cells were seeded in a 6-well plate and then the cells were treated with 100 µg/ml nanoparticles. Cells were fixed with freshly prepared 4% paraformaldehyde (PFA) for 5 min and then washed three times with PBS. The cell nuclei

were then stained with DAPI for 10 min followed by washing three times with PBS. DAPI is bluish colored dye which excites at about 360 nm and emits at about 460 nm when bound to DNA, producing a blue fluorescence. DAPI may also stain RNA (www.vectorlabs.com). Fluorescence imaging was used (Olympus 1X71 inverted fluorescence microscope) in order to study and compare the cellular uptake for two cell lines. [66, 67]

2.4 R11 Peptide Conjugation to Persistent Luminescence Nanoparticles

2.4.1 Materials

Sulfosuccinimidyl 4-(N-maleimidomethyl) cyclohexane-1-carboxylate sodium salt (Sulfo-SMCC), fetal bovine serum (FBS; 10%), Penicillin/Streptomycin, paraformaldehyde (PFA), sterilized phosphate buffered saline (PBS), Sodium Hydroxide (NaOH), L-Cysteine and Trypsin were all purchased form Sigma-Aldrich, $Sr_3MgSi_2O_8:Eu^{2+}$, Dy^{3+} persistent luminescence nanoparticles were synthesized in this lab [20], R11 peptide was provided by professor JT's lab, University of Texas Southwestern Medical Center at Dallas, Ethylenediaminetetraacetic acid (EDTA) was provided by professor Nguyen's lab, University of Texas at Arlington, PC-3 cells (ATCC number CRL-1435), LNCaP cells (ATCC number CRL-1740), Eagle's minimum essential medium (EMEM) and F-12 K medium, were all purchased from ATCC Company. VECTASHIELD® Mounting Medium with PI was purchased from Vector Company. Toluene (mallinckrodt Chemicals Company) and Dimethyl sulfoxide (DMSO) (VWR International) were used as solvents.

2.4.2 Methods

2.4.2.1 Conjugation of R11 Peptide to Persistent Luminescence Nanoparticles

Firstly, the same method for nanoparticles wet grinding (NaOH soaking) and APTES coating, as discussed earlier for folic acid conjugation was used to prepare AG

NPs with NH_2 on the surface to further conjugate with SH group on the surface of R11 peptide. Then, 5mg of the prepared nanoparticles was dissolved in 5ml buffer solution (PBS-2.5 mM EDTA). Then 100µL of Sulfo-SMCC in DMSO (14mM) was added and stirred for 1 hour. Then, 1mg R11 peptide was added and the solution was kept under constant stirring and N_2 gas, for 3 hours at room temperature. Finally, 100µl of 20 mM Cysteine was added to stop the reaction. Subsequently, the prepared nanoparticles were centrifuged and washed 3 times with DMSO and DI water to get rid of unreacted compounds. [6, 16, 55, 75, 76]

Figure 2-6 illustrates the procedure of R11 peptide conjugation to AG NPs by using Sulfo-SMCC as a cross-linker.

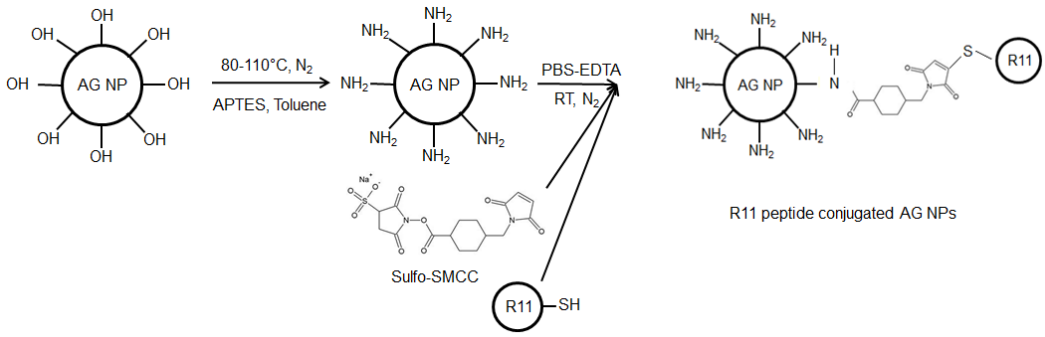

Figure 2-6 Schematic of R11 peptide conjugation to AG NPs

2.4.2.2 Fluorescent Microscopy

PC-3 and LNCaP cells were cultured in F-12 K and EMEM medium, respectively and supplemented with 10% FBS and 1 % penicillin–streptomycin solution at 37°C (5% CO_2). Furthermore, cells were seeded in a 12-well plate and then the cells were treated with 100 µg/ml nanoparticles. Cells were fixed with freshly prepared 4% paraformaldehyde (PFA) for 20 min at room temperature and then washed three times with PBS. Then, 0.02% Triton was used for 5 minutes followed by 3 times PBS washing.

The cell nuclei were then stained with 10μl PI for 10 min followed by sealing the edges of each coverslip with regular transparent nail polish and let it dry for 1 hour. PI is a reddish nuclear counterstain with a broad excitation range at around 535 nm and emission at about 615 nm when bound to DNA (www.vectorlabs.com). Fluorescence imaging was used (Olympus 1X71 inverted fluorescence microscope) in order to study and compare the cellular uptake for two different cell lines as well as two different conjugation methods. [66, 67]

Chapter 3

Results and Discussion

3.1 Folic acid Conjugation to Persistent Luminescence Nanoparticles

3.1.1 FA-NPs Conjugation

As discussed in detail in chapter two, AG NPs were synthesized previously in this lab. Then, wet grinding was used by incorporating NaOH in order to reduce the size and improve the dispersity of the nanoparticles in water solutions, since more OH groups will be coated on the surface of the nanoparticles. Furthermore, APTES coating was used in order to introduce amine (NH_2) groups on the surface of the nanoparticles to be further conjugate to COOH groups of folic acid using the common EDC/NHS method. After washing the nanoparticles for several times to get rid of the unreacted and toxic chemicals, the nanoparticles were ready to do the characterization experiments to study the properties of folic acid conjugated AG NPs as well as cell viability and fluorescent imaging techniques in order to investigate the cellular uptake. The results of these experiments are discussed in detail in the following section.

3.1.2 Fluorescence Spectrophotometer

Photoluminescence excitation and emission spectra of FA-NPs conjugates, AG NPs alone and FA alone dissolved in water and recorded at room temperature are depicted in Figure 3-1. The concentration of the conjugated FA-NPs, AG NPs alone and FA alone was about 3 mg ml^{-1}, 2.325 mg ml^{-1} and 0.625 mg ml^{-1}, respectively. These concentrations were calculated based on conjugation efficiency calculations, which will be discussed in the next section.

As shown in Figure 3-1, FA alone (orange color) excited at 388 nm and 375 nm have the emission at around 450 nm and this result was also confirmed by previous reports. However, the highest intensity of FA is related to excitation and emission about

370 nm and 455 nm respectively. [65, 77, 78] As the photoluminescence intensity for folic acid could be affected by varying the pH [77, 78], all the samples were kept in the same pH (DI water).

In addition, AG NPs alone (blue color) excited at 350 nm showed the emission at 450 nm having very high photoluminescent intensity in solution sample and was previously shown to have higher emission and excitation at the same wavelength when using dry sample (higher concentration). [20]

Finally, the FA-NPs conjugates (green color) were excited at both at 350 nm and 388, which showed two emissions with the same wavelength but different photoluminescent intensity at 450 nm. The 388 nm excitation and the related emission could be attributed to folic acid, whereas, the emission related to excitation at 350 nm could be attributed to AG NPs. As it could be observed, the intensity of folic acid emission increased whereas in the case of AG NPs, it significantly reduced. The pre-conditions for energy transfer from a donor to an acceptor are that the emission of the donor must effectively overlap with the absorption of the acceptor, and the donor and acceptor must be close together with separation less than 10 nm. [65] In this case there is no absorption peak for AG NPs in the range of 200-900 nm, which will be discussed in the next section (UV-vis absorption result). However, from the photoluminescence data it could be seen that there is an excitation around 350 nm for AG NPs which could overlap the emission spectra of folic acid. Also the FA absorption has a peak at 290 and a shoulder between 310-400nm (UV-vis absorption result in the next section), which have a slight overlap with AG NPs emission spectra. However, since the overlap is not significant, the energy transfer is not much probable. In a study by Geszke, Malgorzata, et al. [27], and Manzoor, Koyakutty et al. [25] it was shown that photoluminescent quenching appeared as a process driven by collisions between FA and the QDs and by the strong affinity of

the two carboxylate groups and the nitrogen atoms of FA for zinc atoms on the surface of QDs. Thus, by increasing the concentration of FA the photoluminescent intensity could be decreased. Moreover in a report by Suriamoorthy, Preethi, et al. [65] it was demonstrated that the increase of surface states or defects which were caused during the synthesis process of CdTe QDs, could shorten the luminescence lifetime and quench the luminescence. Thus, it could be possible that the same quenching phenomenon occurred for FA-NPs sample, because of surface defects which were caused during coating and conjugation steps. In addition, more experiments such as luminescent lifetime should be conducted to study the luminescent properties of the FA-NPs and investigate whether energy transfer occurred or not. Obviously, if the luminescence lifetime of the donor is long and that of the acceptor is short, energy transfer can be very efficient. On the contrary, if the luminescence lifetime of the donor is short and that of the acceptor is long, energy transfer would be very inefficient. [65]

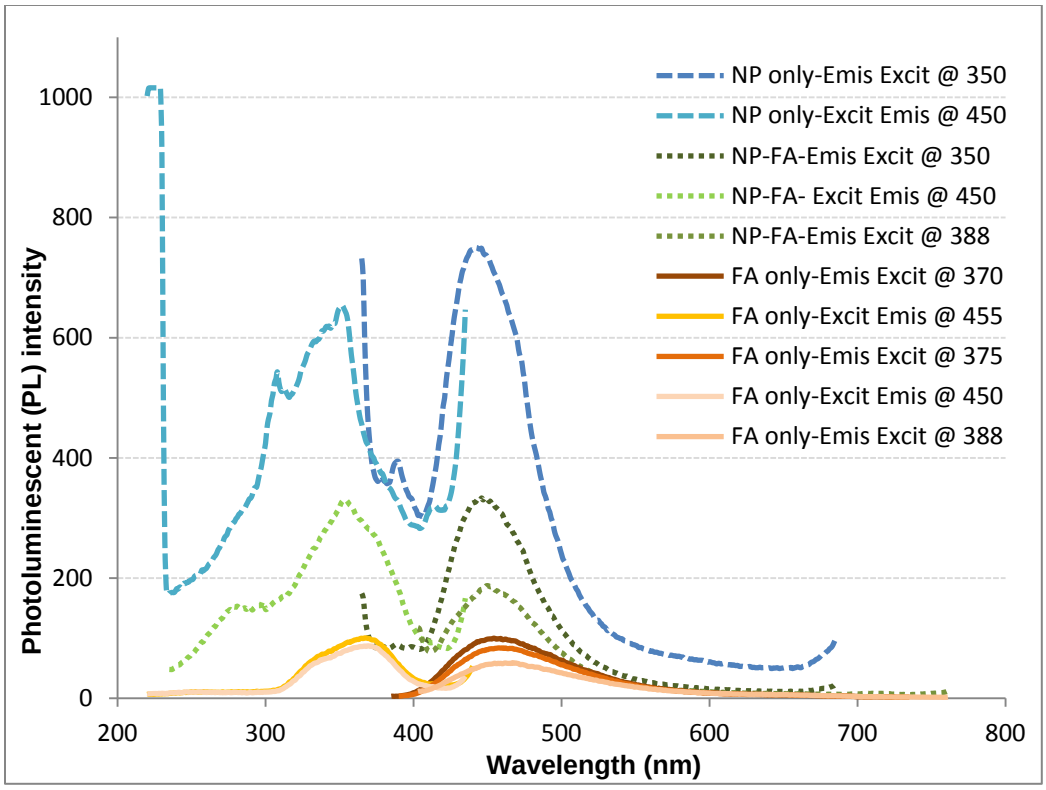

Figure 3-1 Photoluminescence excitation and emission spectra of FA-NPs conjugates (green color), AG NPs (blue color) alone and FA alone (orange color).

Moreover, the reason for choosing the protocol used in this project for FA conjugation was that the afterglow properties should be maintained during and after the conjugation procedure, as these nanoparticles have the potential to be conjugated to photosensitizer and be efficiently used in PDT applications. [20-23] Figure 3-2 illustrates the fluorescence and afterglow properties of the conjugated AG NPs to folic acid using two different methods, under UV lamp. As shown in Figure 3-2 (A) the afterglow properties disappeared by using MES buffer (pH=6) solution instead of DMSO, to conjugate FA to AG NPs. Therefore it could be concluded that maybe the acidity environment of MES buffer solution could affect the luminescent and afterglow properties

because of the change on surface defects of the nanoparticles during conjugation process, and this was also reported and confirmed in other studies. [20, 64] However, as shown in Figure 3-2 (B) the FA conjugated AG NPs could maintain the fluorescent and afterglow properties using the same method for conjugation as discussed in chapter two (DMSO as a solvent).

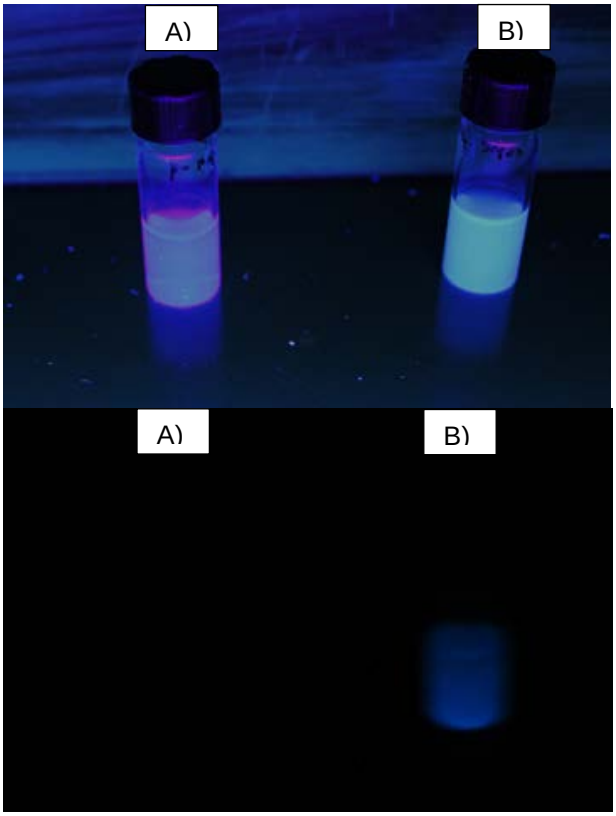

Figure 3-2 Fluorescence and afterglow properties of AG NPs conjugated to folic acid, under UV lamp (A) MES method, (B) DMSO method

3.1.3 UV-Vis Absorption Spectrophotometer

Figure 3-3 illustrates the absorption spectra of AG NPs alone, FA conjugated AG NPs and different concentrations of FA alone. The concentration of the conjugate and AG

NPs alone was maintained at 125 µg ml^{-1} and FA alone was measured in five different concentrations including 62.5, 46.874, 31.25, 23.437 and 15.625 µg ml^{-1}.

AG NPs alone did not show any peak in the range of 200 nm to 1100 nm. However, FA alone showed a sharp peak at about 290 nm and a broader peak at 345 nm. In addition, the FA conjugated Ag NPs showed similar peaks to FA alone, even though the peaks, especially the broader one, shifted a little bit to higher wavelengths. Thus, these results could confirm the successful conjugation of FA to AG NPs, when comparing the existence of FA peaks in conjugated sample to AG NPs alone, which did not show any peaks in that range. This method was also used by another study to confirm the FA conjugation to upconversion luminescence nanoparticles. [64] Notably, UV characterization could be effectively used to confirm the conjugation of biomolecules. However it requires precise purification and washing of the material to make sure that there are no free molecules that could confound the analysis. In this project, the conjugated samples were centrifuged and washed more than three times to make sure that there was no free FA inside the solutions. [79]

Moreover, absorption spectra illustrated in Figure 3-3 was used to calculate the conjugation efficiency of FA to AG NPs. As previously mentioned, five different concentrations of FA was used to plot a standard curve for the sharp peak of FA at 292 nm, as depicted in Figure 3-4, the linear equation resulted from the standard curve, could be used to calculate the concentration of FA in FA-NPs sample, by using the absorbance intensity of the conjugated sample. Therefore, the conjugation efficiency would be 28.053 µg FA per 125 µg AG-FA NPs. In addition, other concentration-dependent methods such as FTIR could be used to calculate the conjugation efficiency. [80]

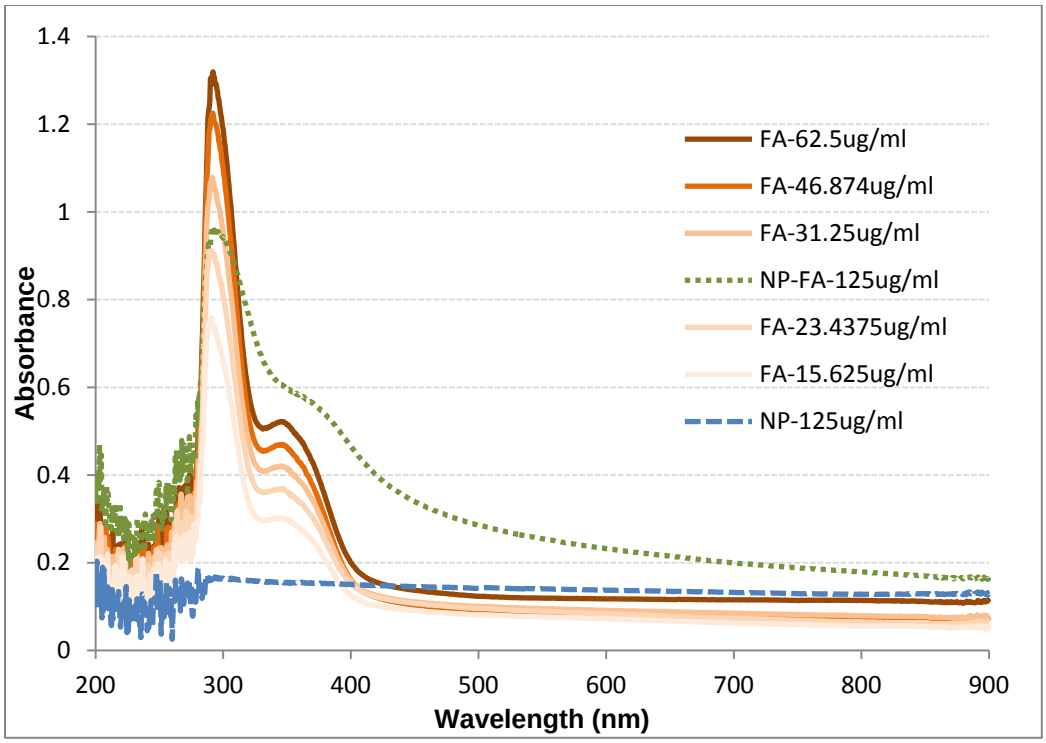

Figure 3-3 Absorption spectra of AG NPs alone (blue color), FA conjugated AG NPs (green color) and different concentrations of FA alone (orange color)

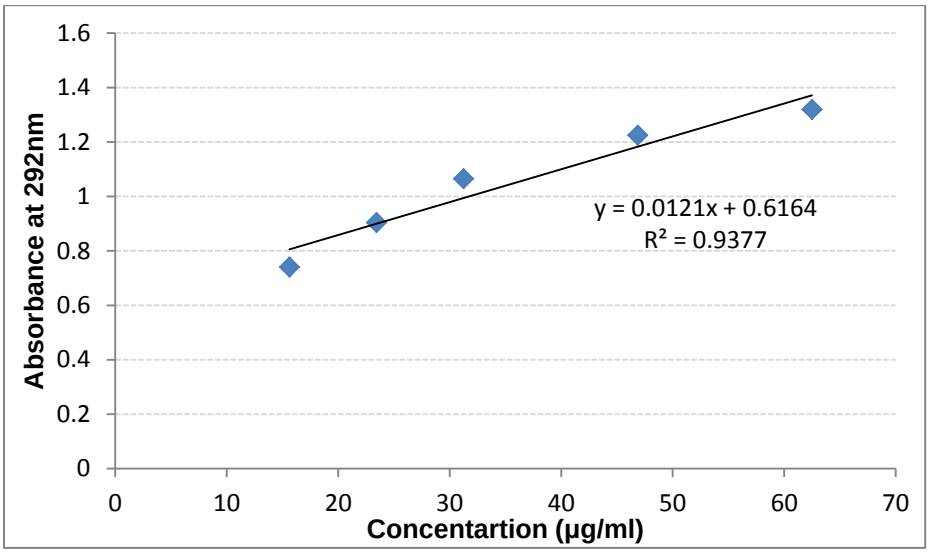

Figure 3-4 Standard curve for the FA sharp peak at 292 nm

3.1.4 Dynamic Light Scattering (Zeta Potential and Size)

Firstly, dynamic light scattering (DLS) was used to measure the zeta potential (surface charge), in order to study the stability of the nanoparticles as well as confirming the FA conjugated to the nanoparticles. All samples were dissolved in DI water and kept at the same concentrations (0.5 mg ml^{-1}). Table 3-1 summarizes the results of zeta potential for different samples and Figure 3-5 illustrates the zeta potential change before and after conjugation to folic acid. The AG NPs alone showed the surface charge of -24.85 mV, which could be attributed to the OH groups on the surface of the nanoparticles introduced during synthesis. [20] After wet grinding and NaOH soaking for 24 hours, the zeta potential showed relatively more negative results, because of more OH groups introduced by this process. However, After APTES coating, the negative surface charge could be replaced by more positive NH_2 groups on the surface of the nanoparticles, resulting in the zeta potential of -12.64 mV. The more efficient APTES coating could result in more positive charge on the surface of the nanoparticles. Finally, after conjugation with folic acid the zeta potential increased slightly due to the negative charge introduced by ionization of the a-carboxylic group. [27, 62] It seems that water dispersity improved and this could be due to higher charge density in the case of nanoparticles as compared to microparticles.

Table 3-1 Zeta potential comparison

Sample	Zeta potential (mV)
AG NPs	-24.85±0.94
AG NPs soaked in NaOH for 24 hours	-27.26±1.11
AG NPs soaked in NaOH for 24 hours And APTES coating	-12.64±0.83
AG NPs soaked in NaOH for 24 hours and APTES coating conjugated to FA	-30.40±0.44

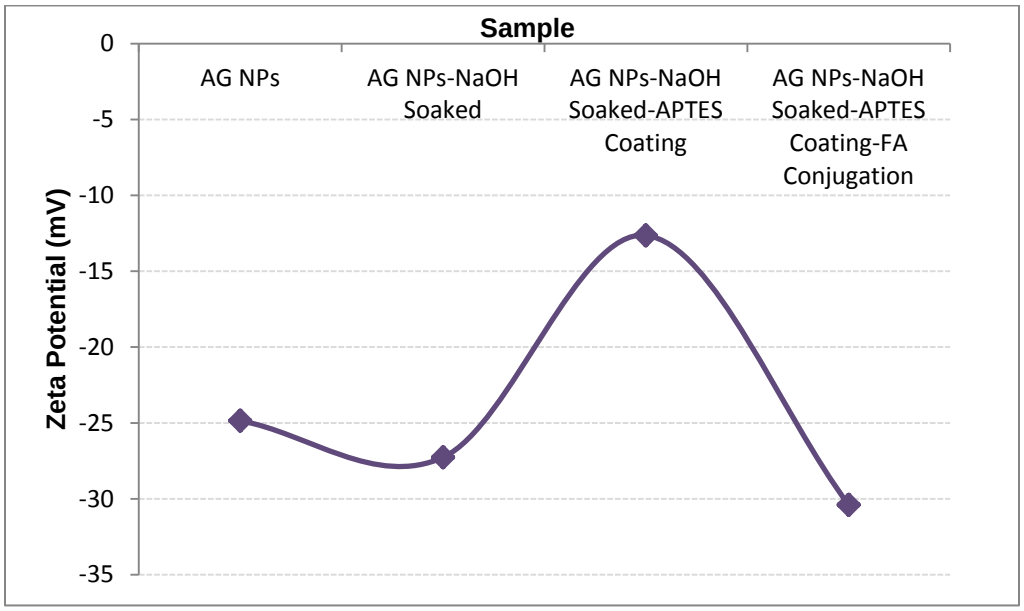

Figure 3-5 Zeta potential change for different samples

Secondly, DLS was used to study the effect of conjugation on the size of AG NPs. Table 3-2 and Figure 3-6 shows the results for size improvement after the FA conjugation. As it is clearly shown, the size of nanoparticles decreased almost two times after NaOH soaking method (as was previously used by another group to obtain nanometer sized particles [56]) and FA conjugation. Also, filtration could be an effective way to reduce the size. Thus, the size of the AG NPs reduced from 1296.8 nm to 543.2

nm after NaOH soaking, FA conjugation and filtration by 1 μm pore size filtration paper. In order to improve the size even more, further experiments should be conducted to control the APTES coating efficiency as well as FA conjugation efficiency. Moreover, using smaller pore size filtration paper could further improve the size of the nanoparticles into the desired range.

Table 3-2 Size improvement

Sample	Size (nm)
AG NPs	1296.8±289.9
AG NPs soaked in NaOH for 24 hours and APTES coating conjugated to FA	707.45±45.4
AG NPs soaked in NaOH for 24 hours and APTES coating conjugated to FA, filtered by 1 μm pore size filtration paper	543.2±10.3

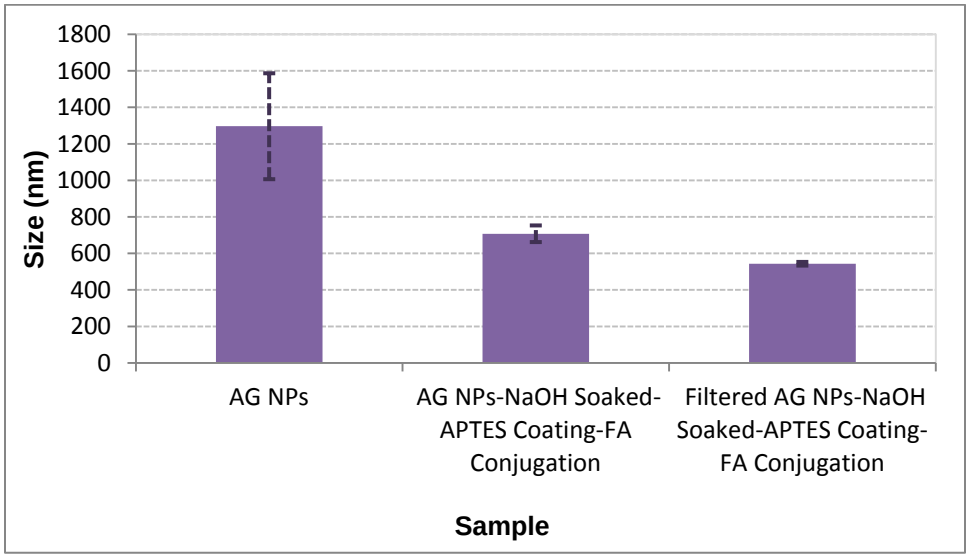

Figure 3-6 Size improvement after NaOH soaking, FA conjugation and filtration

3.1.5 Cell Viability

The cytotoxicity of AG NPs and FA-NPs under in vitro conditions in prostate (PC-3) was examined in terms of the effect of those nanoparticles on cell proliferation by the MTT assay [32, 81-83]. Untreated cells (PBS-negative control) as well as cells treated with 62.5, 125, 250, 500, μg ml^{-1} concentrations of the prepared nanoparticles for 24 h were subjected to the MTT assay for cell viability determination. In this assay, only cells that are viable after 24 h exposure to the sample are capable of metabolizing a dye (3-(4,5-dimethylthiazol- 2-yl)-2,5-diphenyltetrazolium bromide) efficiently and produce purple colored crystals which are dissolved in a detergent and analyzed by spectrophotometer. After 24 h of post treatment, PC-3 cells showed excellent viability even up to 500 μg ml^{-1} concentrations of the FA conjugated AG NPs (Figure 3-7). However, AG NPs alone showed a relative amount of toxicity at the highest concentration (500 μg ml^{-1}), but maintained the viability for lower concentrations. [81]

These results clearly demonstrated that FA conjugation provide a non-toxic coating on AG NPs nanoparticles and corroborate the results as seen in the cellular uptake studies which will be discussed in the following section.

Furthermore, in another study performed in this lab [20] it was demonstrated that these AG NPs also did not show any toxicity to PNT1A human normal prostate epithelium cells.

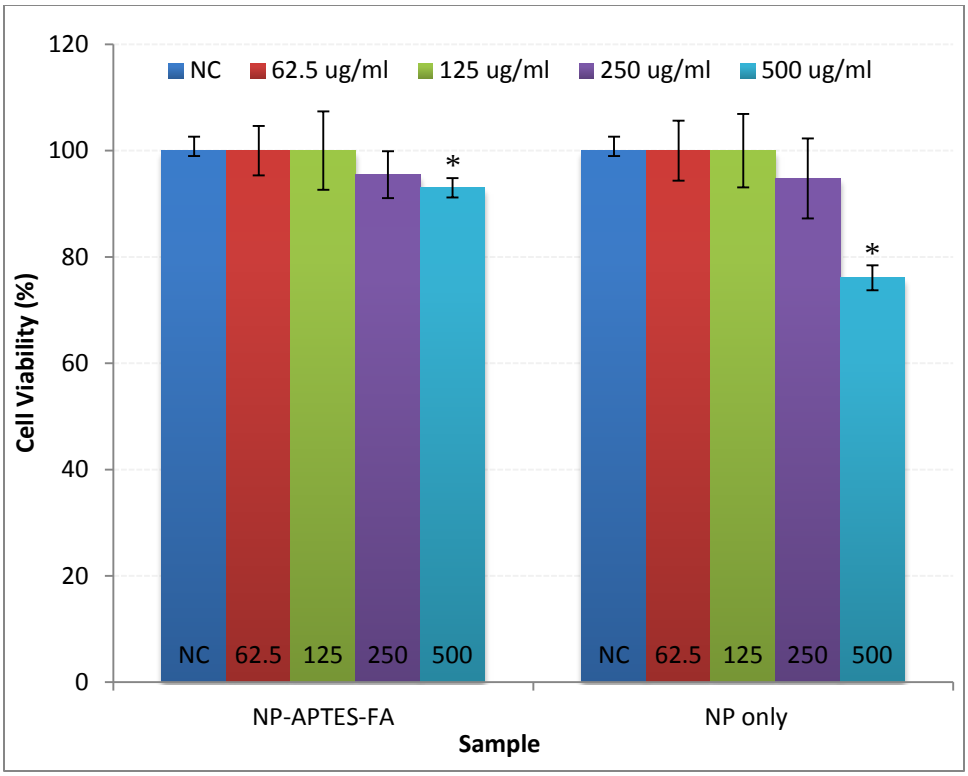

Figure 3-7 Cell viability enhancement for conjugated FA NPs using MTT assay

(*: $P < 0.05$)

3.1.6 Fluorescent Imaging

In this project, in vitro fluorescent imaging was performed using the PC-3 cell lines as FA receptor negative [35], MCF-7 cell lines as FA receptor positive (slightly) [32, 34, 36-38] and KB cells as FA positive [32, 37] to study and compare the cellular uptake and target recognition capability of FA conjugated AG NPs which limit the non-receptor mediated endocytosis of these nanoparticles when incorporated without FA conjugation. Figure 3-8 illustrates the result of the fluorescent imaging. The first top row shows the bright field images which illustrate the cells morphology and also FA-NPs which were uptaken by three kinds of cells. The second top row shows the nucleus staining with PI

which has the emission around 625 nm when excited at 535 nm. The next row shows the FA-NPs fluorescent which has the emission of 450 nm when excited at 350 nm. Finally the last row shows the merged images of the second and third rows. The images were taken at 20x magnification. As it is clearly shown in bright field, FA-NPs and merge images, the cellular uptake of MCF-7 and KB cells (FA receptor positive) have been improved as compared to PC-3 cells (FA receptor negative). In addition, it seemed that KB cells had higher uptake in comparison with MCF-7 cells, since KB cells express a higher amount of FA receptor than the MCF-7 cells. The higher uptake of KB cells and also MCF-7 cells should be attributed to the highly specific interaction between FA on the FA-NPs and FA receptor on the KB and MCF-7 cells resulting in more efficient internalization of the FA-NPs into the cells via FR-mediated endocytosis, which promoted the entry of the FA-NPs into FA receptor-overexpressed MCF-7 and KB cells. Other reports demonstrated quite similar results and confirmed the results in this research project for folic acid conjugation. [32, 34-38] Since, investigating the cellular uptake by fluorescent imaging is a common method but it is qualitative, future work could be conducted using other methods to investigate the cellular uptake quantitatively (fluorescent intensities measurements). [84, 85]

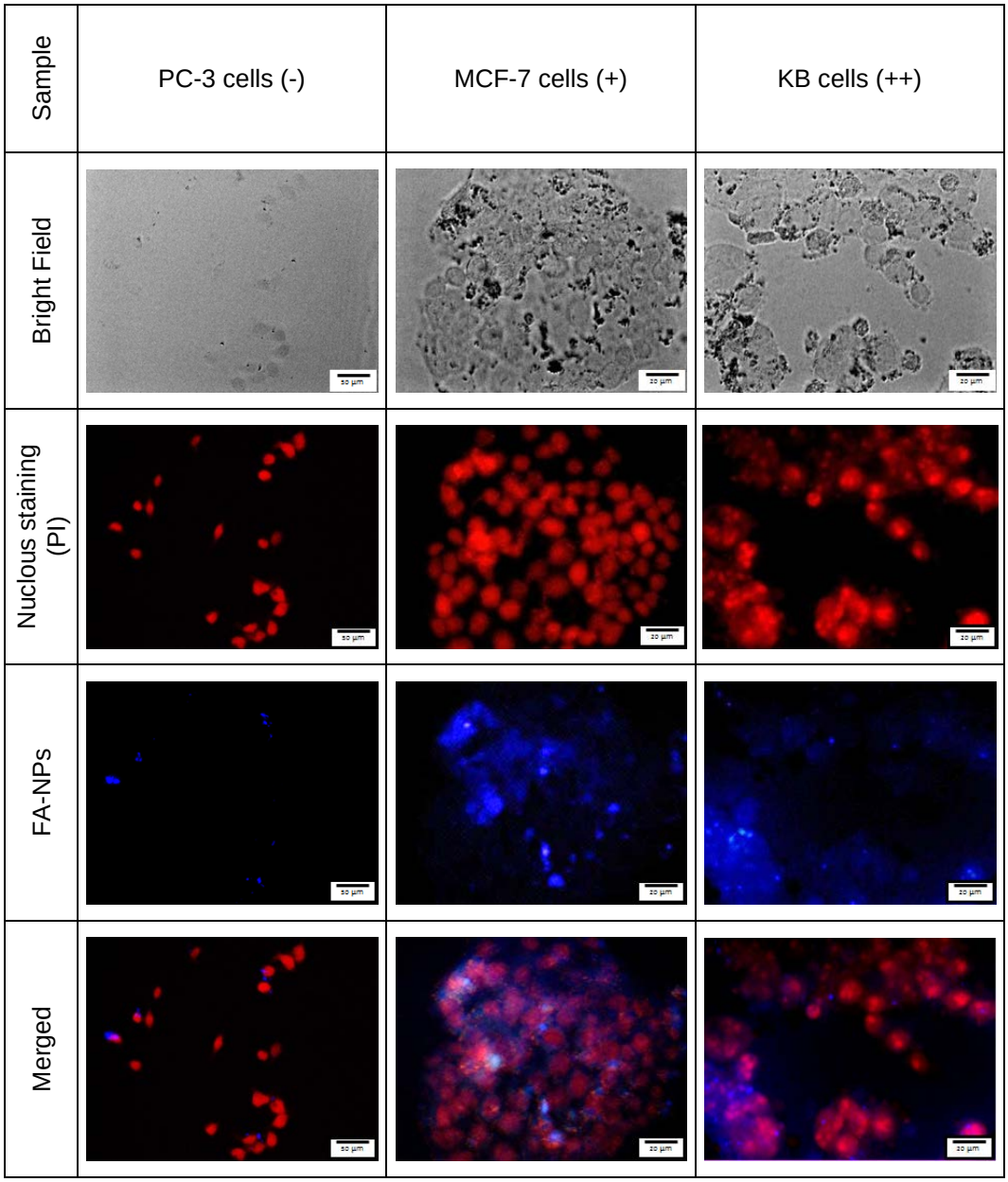

Figure 3-8 Fluorescent imaging and cellular uptake comparison for PC-3, MCF-7 and KB cell lines: Top row: Bright field, Second row: Nucleus staining with PI, Third row: Conjugated FA-NPs fluorescence, Bottom row: Merge of second and third row. 20X magnification

3.2 RGD Peptide Conjugation to Persistent Luminescence Nanoparticles

3.2.1 RGD-NPs Conjugation

As discussed in detail in Chapter 2, AG NPs were synthesized previously in this lab. Then, wet grinding was used by incorporating NaOH in order to reduce the size and improve the dispersity of the nanoparticles in water solutions as more OH groups will be coated on the surface of the nanoparticles. Furthermore, APTES coating was used in order to introduce amine (NH_2) groups on the surface of the nanoparticles to be further conjugate to COOH groups of RGD peptide using the common EDC/NHS method. In addition, plasma coated Ag NPs were also used to be conjugated to amine groups (NH_2) of the RGD peptide by incorporating another method using EDC/NHS chemistry and MES as buffer solution. After washing the nanoparticles for several times to get rid of the unreacted and toxic chemicals, the nanoparticles were ready to do the fluorescent imaging techniques in order to investigate and compare the cellular uptake. The results of these experiments are discussed in detail in the following section.

RGD peptide is more specific to breast cancer cells, as compared to folic acid which can be efficiently targeted to variety of cancer cells, Thereby it could be a promising candidate for breast cancer diagnosis and therapy. [30, 44]

Recent studies showed that $\alpha_v\beta_3$ functions differently on various cell types. It could mediate endothelial cell migration and survival during angiogenesis when expressed on activated endothelial cell surface and it could facilitates blood vessel invasion by tumor cells during metastasis when expressed on tumor cells. $\alpha_v\beta_3$ binds to ECM proteins via the RGD peptide sequence; therefore, RGD peptides and their derivatives can serve both as integrin inhibitors to induce endothelial cell apoptosis and inhibit angiogenesis and also integrin-targeted probes for monitoring tumor angiogenic

and metastatic activities. Thus, peptide ligands for Integrin $\alpha_v\beta_3$ are well known markers of tumor angiogenesis [82, 86, 87]

3.2.2 Fluorescent Imaging (Method 1 and 2)

In this project, in vitro fluorescent imaging was performed using MCF-7 cell lines (integrin $\alpha_v\beta_3$ negative) and MDA-MB-231 cell lines (integrin $\alpha_v\beta_3$ positive) [41-43] to study and compare the cellular uptake and to determine whether the uptake is integrin $\alpha_v\beta_3$ expression level dependent. [82]

Figure 3-9 and Figure 3-10 illustrates the result of the fluorescent imaging for method 1 [59, 62] which was carried out using EDC/NHS chemistry in DMSO as a solvent and method 2 [70-72] which was performed using the same EDC/NHS method but by replacing DMSO with MES buffer solution and plasma coated AG NPs instead of AG NPs. The first top row shows the bright field images which illustrate the cells morphology and also RGD-NPs which were uptaken by two kinds of cells. The second top row shows the nucleus staining with PI which has the emission around 625 nm when excited at 535 nm. The next row shows the RGD-NPs fluorescent which has the emission of 450 nm when excited at 350 nm. Finally the last row shows the merge images of the second and third rows. The images were taken at 20x magnification. As depicted in the figure, bright field, RGD-NPs and merge images, the cellular uptake of MDA-MB-231 cells (RGD peptide receptor positive) have been improved quite significantly as compared to MCF-7 (RGD peptide receptor negative). [41-43, 88] Other studies also demonstrated similar results for these cell lines because of the low level of integrin $\alpha_v\beta_3$ on MCF-7 cell membrane, thereby the uptake of cRGD modified AG NPs into MCF-7 cells was few after the 24-h incubation period in comparison with the other cell line, MDA-MB-231, which has high level of integrin $\alpha_v\beta_3$ on their cell membranes. [42]

Finally, by comparing the results for method 1 and 2, for the conjugation of RGD peptide to AG NPs, it seems that method 2 (MES method) showed relatively higher cellular uptake than method 1 (DMSO) method, especially in bright filed images. However, as discussed in Section 3.1.2, acidity environment resulting in change of nanoparticles surface defects could affect the photoluminescence and afterglow properties of AG NPs limiting the application of these nanoparticles for photodynamic therapy. [20] Thus, method 1 which showed both promising results for cellular uptake as well as maintaining afterglow and florescent properties after conjugation to RGD peptide could be effectively used in targeted cancer diagnosis and therapy applications.

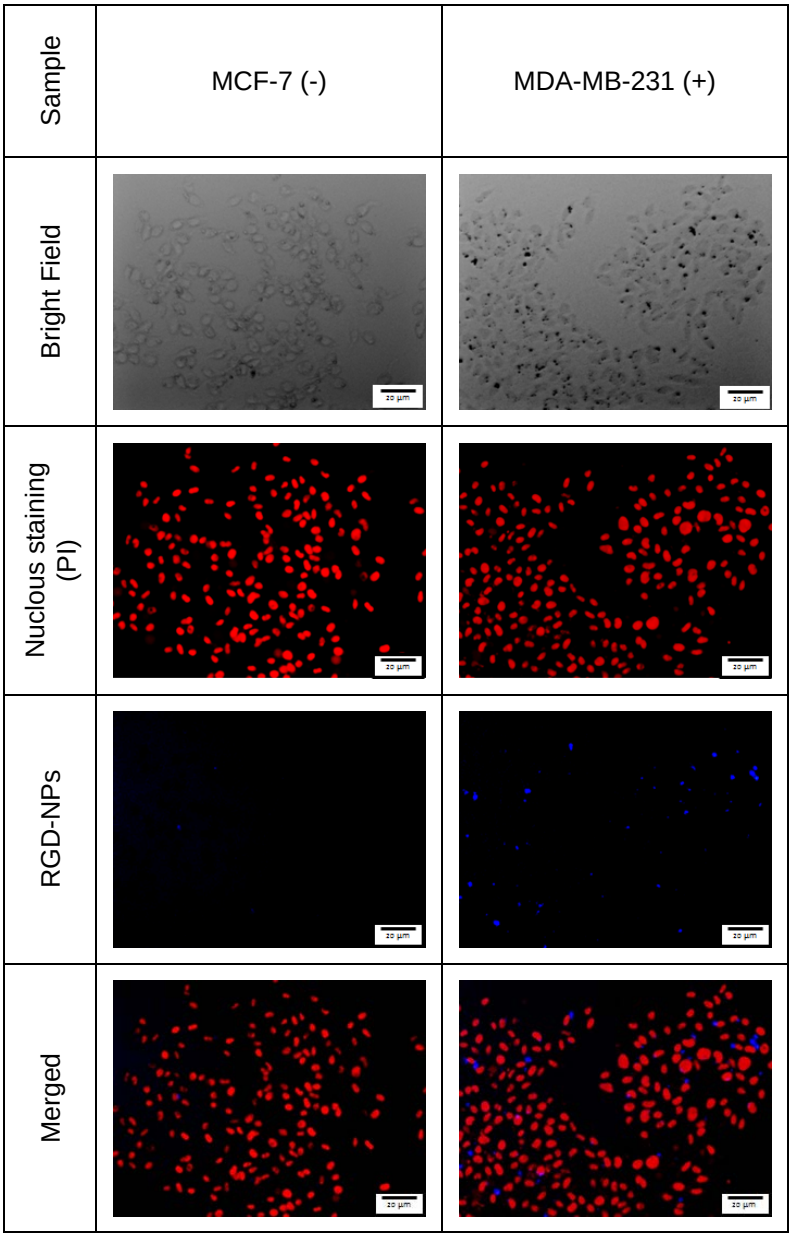

Figure 3-9 Fluorescent imaging and cellular uptake comparison for MCF-7 and MDA-MB-231 cell lines (method 1): Top row: Bright field, Second row: Nucleus staining with PI, Third row: Conjugated RGD-NPs fluorescence, Bottom row: Merge of second and third row. 20X magnification

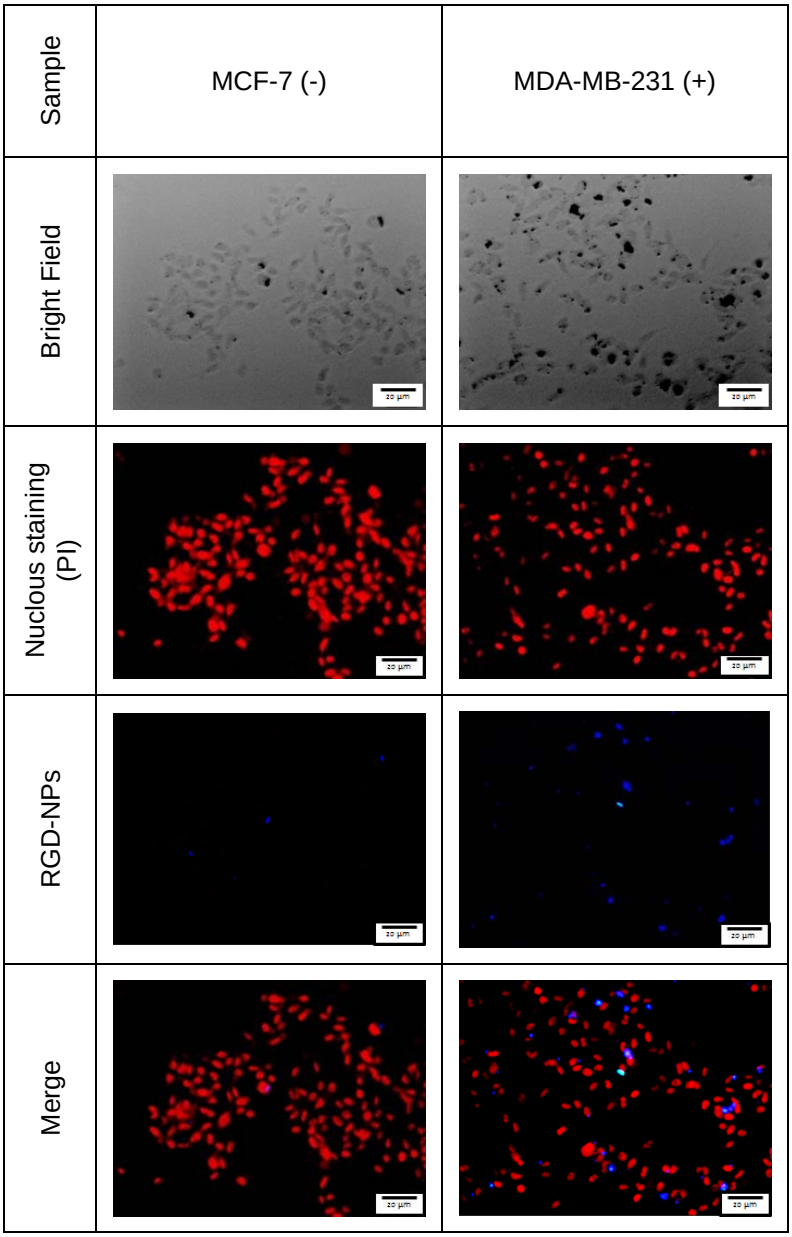

Figure 3-10 Fluorescent imaging and cellular uptake comparison for MCF-7 and MDA-MB-231 cell lines (method 2): Top row: Bright field, Second row: Nucleus staining with PI, Third row: Conjugated RGD-NPs fluorescence, Bottom row: Merge of second and third row. 20X magnification

3.3 PSMA Inhibitor Conjugation to ZnS:Mn Luminescent Nanoparticles

3.3.1 PSMA Inhibitor-NPs Conjugation

As discussed in detail in Chapter 2, ZnS:Mn NPs were synthesized previously in this lab. During synthesis, amine (NH_2) groups were introduced on the surface of the nanoparticles to be further conjugate to COOH groups of PSMA inhibitor by incorporating the common EDC/NHS method using three solvents. After washing the nanoparticles for several times to get rid of the unreacted and toxic chemicals, the nanoparticles were ready to do the fluorescent imaging techniques in order to investigate and compare the cellular uptake. The results of these experiments are discussed in detail in the following section.

Inhibitors of NAALADase (PSMA) which was used in this research, could strongly bind to PSMA, thereby this targeting biomolecule could be efficiently and specifically used for prostate cancer diagnosis and therapy. This biomolecule could introduce new avenues for prostate cancer applications, as it is more specific to prostate cancer cells as compared to folic acid and RGD peptide, which were discussed in detail in previous sections. [54, 82]

3.3.2 Fluorescent Imaging

In this project, in vitro fluorescent imaging was performed using PC-3 cell lines (PSMA inhibitor negative) and LNCaP cell lines (PSMA inhibitor positive) [47, 50-53] to study and compare the cellular uptake and to determine whether the uptake is PSMA expression level dependent.

Figure 3-11 and Figure 3-12 illustrates the result of the fluorescent imaging for method 1 [46, 48, 52] which was carried out using EDC/NHS chemistry in DI water as a solvent and method 2 [73] which was performed using the same EDC/NHS method but with replacing DI water with PBS buffer solution. The first top row shows the bright field

images which illustrate the cells morphology and also PSMA inhibitor conjugated ZnS:Mn NPs (PSMAi-NPs) which were uptaken by two kinds of cells. The second top row shows the nucleus staining with DAPI which has the emission around 360 nm when excited at 460 nm. The next row shows the PSMAi-NPs fluorescent which has the emission of 600 nm when excited at 350 nm. The images were taken at 20x magnification. It could clearly be observed that for PSMAi-NPs the cellular uptake of LNCaP cells (PSMA receptor positive), shown in fluorescent images (merge), have been improved quite significantly as compared to PC-3 (PSMA receptor negative). Other studies also demonstrated similar results for these cell lines. The LNCaP human prostate epithelial cells express a high level of PSMA protein on their cell membrane, which could represent a good model for in vitro and in vivo prostate cancer studies. However, PC-3 human prostate epithelial cells normally do not express any detectable levels of the PSMA protein. [47, 50-53]

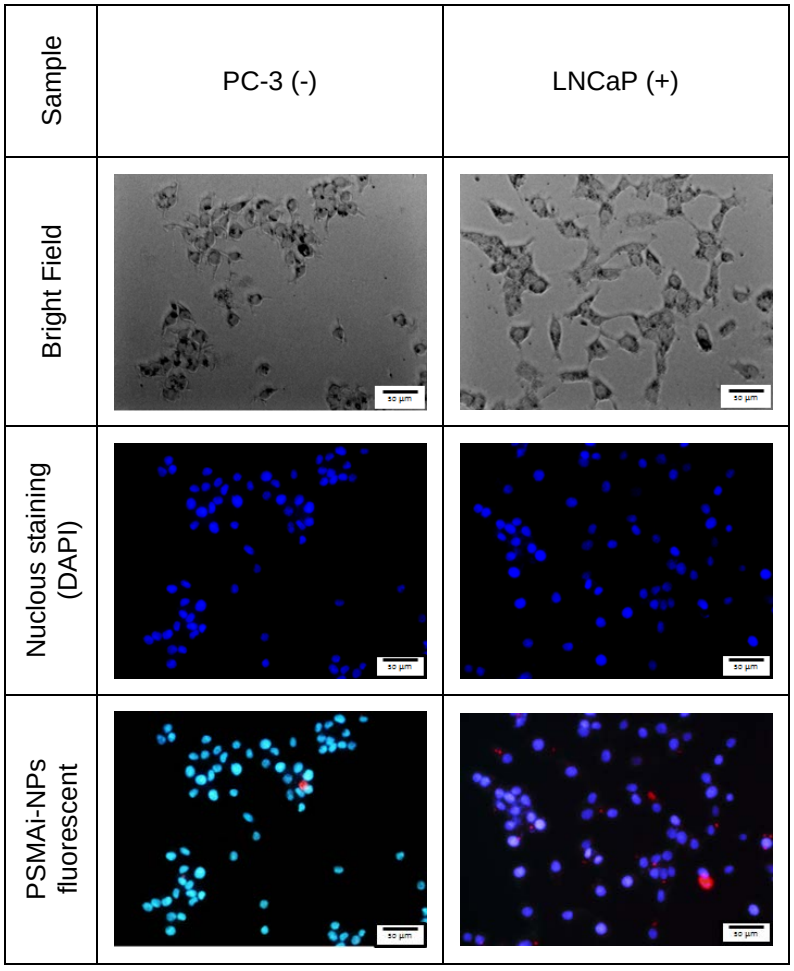

Figure 3-11 Fluorescent imaging and cellular uptake comparison for PC-3 and LNCaP cell lines (method 1): Top row: Bright field, Second row: Nucleus staining with DAPI, Bottom row: PSMAi-NPs fluorescent and DAPI staining. 20X magnification

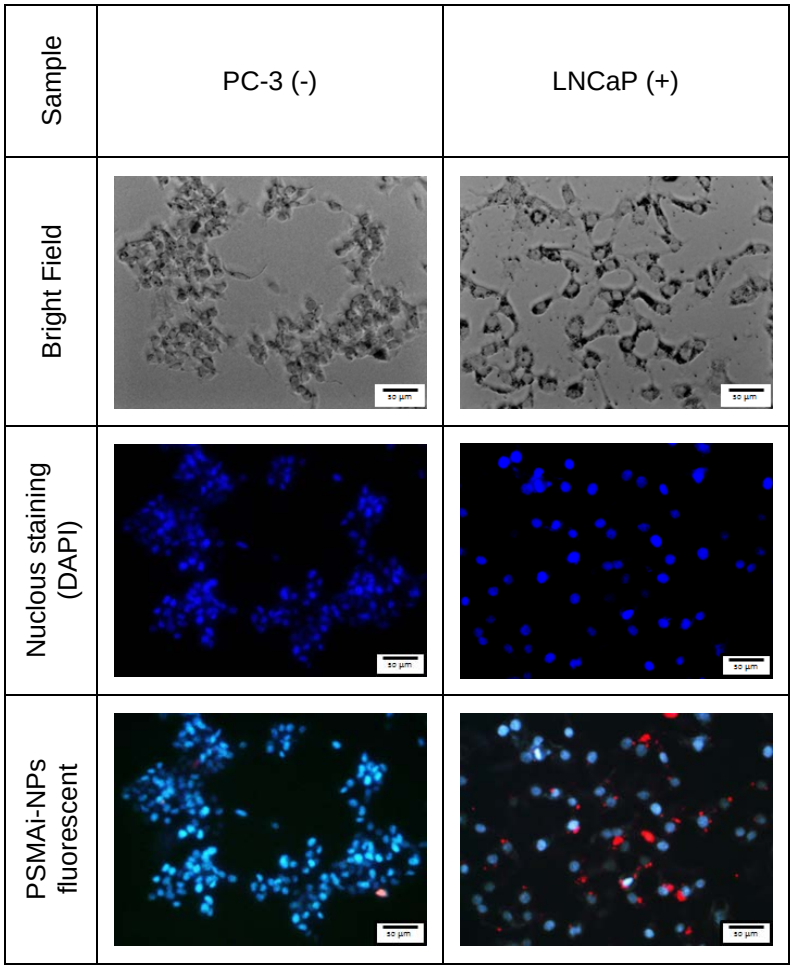

Figure 3-12 Fluorescent imaging and cellular uptake comparison for PC-3 and LNCaP cell lines (method 2): Top row: Bright field, Second row: Nucleus staining with DAPI, Bottom row: PSMAi-NPs fluorescent and DAPI staining. 20X magnification

Finally, by comparing the results for LNCaP cells, using the methods 1, 2 and 3 for conjugation of PSMA inhibitor to ZnS:Mn NPs (discussed in detail in chapter 2), which are depicted in Figure 3-13, it seems that method 2 (PBS method) showed relatively higher cellular uptake than method 1 and 3 (DI water method and MES method), especially in fluorescent images. Although, the fluorescent properties seemed to be

maintained as contrast to RGD peptide conjugated AG NPs which lost their afterglow and fluorescent properties to some extent, but the cellular uptake and red fluorescent did not improve when using MES buffer instead of PBS buffer and this could be due to the change on surface defects of nanoparticles caused by acidity environment. Also by comparing method 1 and 2, it seems that pH has some effect on conjugation process and cellular uptake, thereby, since there was no control on the pH of DI water, the cellular uptakes seems to be less than method 2, which PBS buffer was used as a solvent.

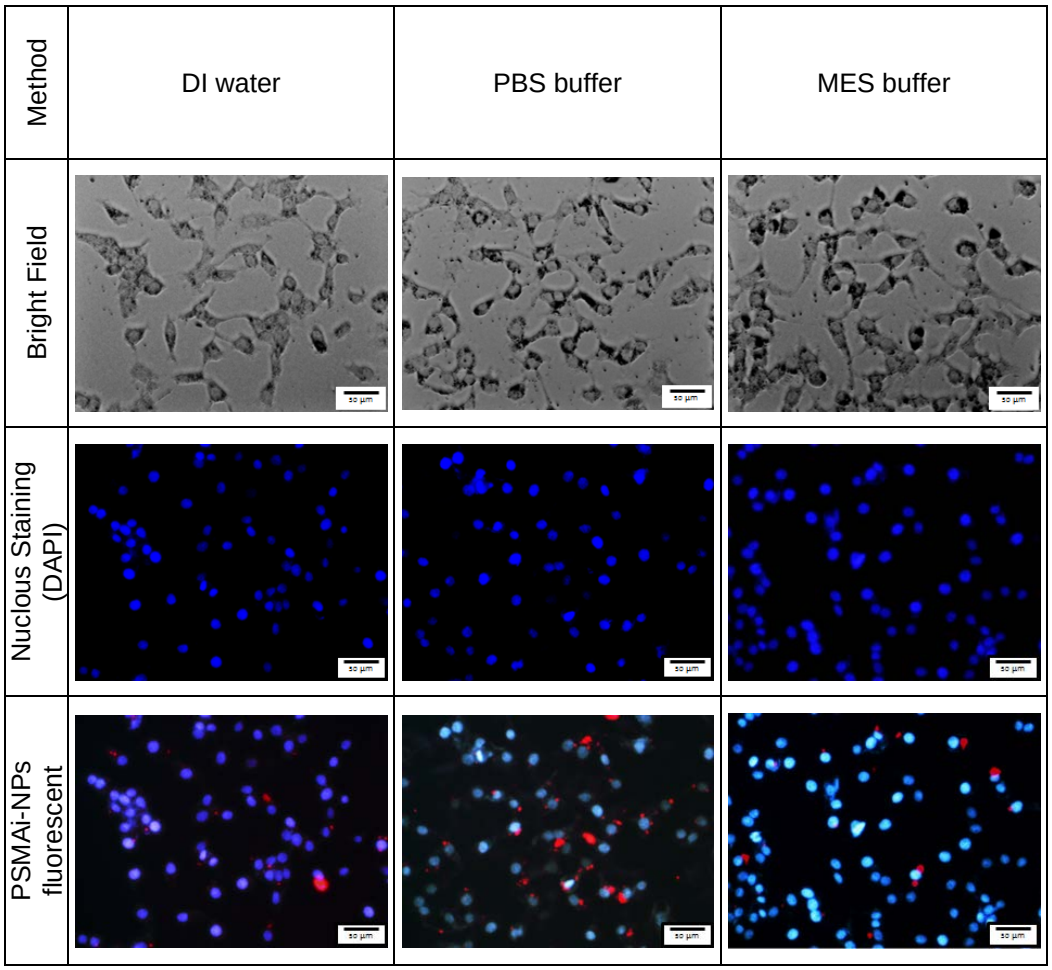

Figure 3-13 Comparison of fluorescent imaging and cellular uptake for LNCaP cell lines by using three methods for conjugation: DI water (method 1), PBS buffer (method 2), MES buffer (method 3). Top row: Bright field, Second row: Nucleus staining with DAPI, Bottom row: PSMAi-NPs fluorescent and DAPI staining. 20X magnification

3.4 R11 peptide Conjugation to Persistent Luminescence Nanoparticles

3.4.1 R11-NPs Conjugation

As discussed in detail in Chapter 2, AG NPs were synthesized previously in this lab. Then, wet grinding was used by incorporating NaOH in order to reduce the size and improve the dispersity of the nanoparticles in water solutions as more OH groups will be coated on the surface of the nanoparticles. Furthermore, APTES coating was used in order to introduce amine (NH_2) groups on the surface of the nanoparticles to be further conjugate to SH groups of R11 peptide using the common sulfo-SMCC as an intermediate. After washing the nanoparticles for several times to get rid of the unreacted and toxic chemicals, the nanoparticles were ready to do the fluorescent imaging techniques in order to investigate and compare the cellular uptake. The results of these experiments are discussed in detail in the following section.

R11 peptide is a novel biomolecule which is known to be more specific to prostate cancer cells, as compared to RGD peptide folic acid, Thereby it could be a promising candidate for prostate cancer diagnosis and therapy. [6, 89]

3.4.2 Fluorescent Imaging

In this project, in vitro fluorescent imaging was performed using two prostate cancer cell lines, PC-3 and LNCaP, to study and compare the cellular uptake and to investigate enhanced targeted internalization of R11-NPs to NPs alone. [6, 16, 55]

Figure 3-14 illustrates the result of the fluorescent imaging for R11-NPs and NPs alone without any conjugation to R11 peptide.

The first two top rows show the result for conjugated R11-NPs which were uptaken by two kinds of cells. The two bottom rows show the results of PC-3 and LNCaP cells treated with NPs alone. The nucleus staining was done using PI which has the

emission around 625 nm when excited at 535 nm. The images were taken at 20x magnification.

As it is shown in Figure 3-14 the R11-NPs samples showed higher uptake for both PC-3 cells and LNCaP cells as compared to NPs alone without conjugation to R11 peptide. Moreover, although by comparing the results shown in Figure 3-14, the cellular uptake of R11-NPs did not seem to be changed for PC-3 and LNCaP cells (very close uptake but maybe a little higher for LNCaP cells when observed qualitatively under microscope), other results for different sections of the samples under the microscope (Figure 3-15) showed higher uptake for LNCaP cells as compared to PC-3 cells. Also in a study by Wadajkar, Aniket S., et al [6], higher uptake of R11-PMNPs than PMNPs alone by PC3 and LNCaP cells was observed which is also probable in this project. In addition, higher nanoparticle uptake by LNCaP cells as compared with those of PC3 cells was reported. Also, it was shown that the extent of cellular uptake of the nanoparticles is dependent on several factors including type of cells, presence of cell surface markers, hydrophilicity/hydrophobicity level of nanoparticles, surface properties of the nanoparticles, and cell-nanoparticle interaction.

In another study, it seemed that PC-3 cells had much rapid uptake rate than the other prostate cancer cells, thereby in 30 minutes, PC-3 showed relatively higher uptake as compared to LNCaP cells. [55]

Thus to confirm the results in this project for comparison of cellular uptake for PC-3 and LNCaP cells, quantitative studies could further be conducted.

In another study, it was shown that oligoarginine peptide (i.e., R11) appears to have high affinity to prostate cancer cells compared with other peptides tested. In addition R11 was developed as an imaging probe to detect prostate cancer. It was shown that the uptake of R11 is mediated through macropinocytosis. It was concluded that the

laminin receptor is one of the initial binding sites responsible for R11 peptide uptake in prostate cells. This indicates that the R11 peptides show greater specificity toward prostate cancer cells compared to other CPPs. [16]

Consequently, other studies should be performed to investigate the mechanism of uptake and amount of laminin receptor on PC-3 and LNCaP cells to compare the cellular uptake for those cell lines.

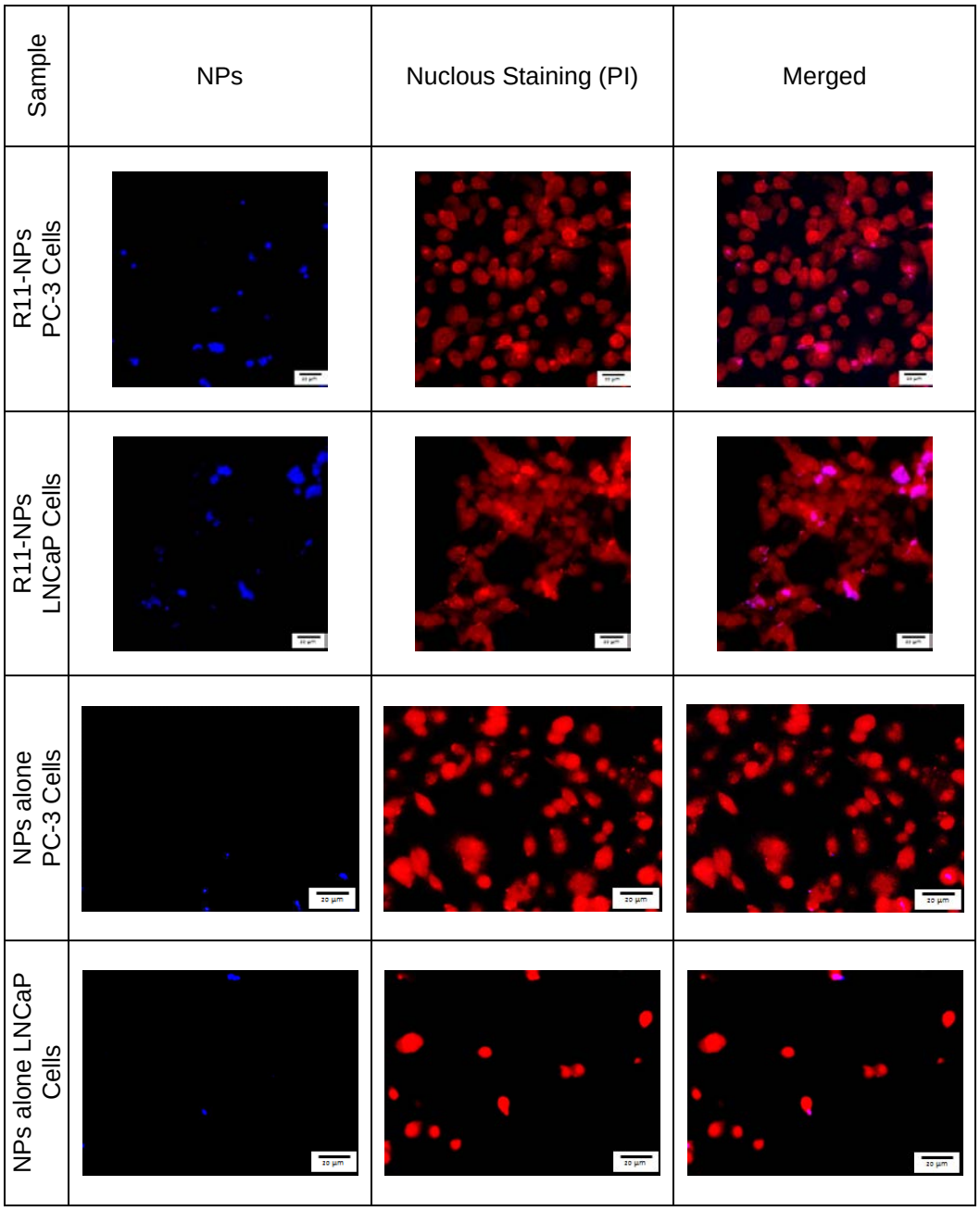

Figure 3-14 Comparison of fluorescent imaging and cellular uptake for PC-3 and LNCaP cell lines by using two different samples: (First two top rows: Conjugated R11-NPs), Last two bottom rows: NPs alone 20X magnification

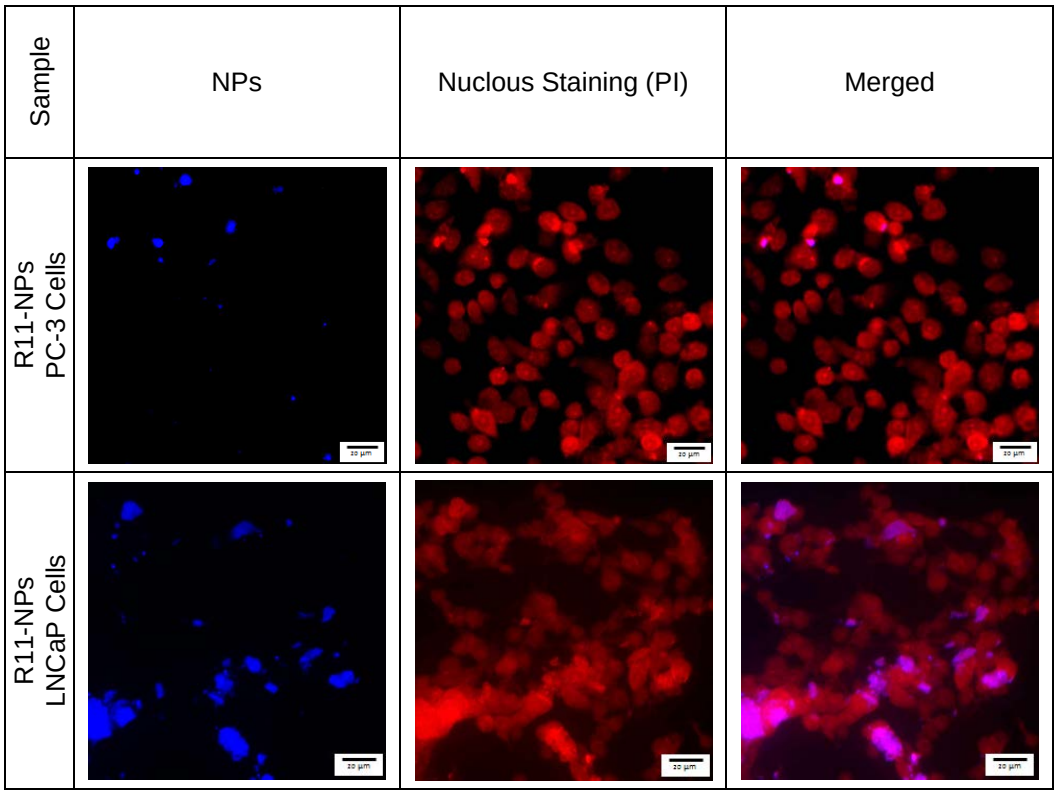

Figure 3-15 Comparison of fluorescent imaging and cellular uptake for PC-3 and LNCaP cell lines by using Conjugated R11-NPs, 20X magnification

Chapter 4

Conclusion and Future Works

4.1 Summary

Inorganic nanoparticles have attracted much attention in the recent decades as potential diagnostic and therapeutic systems in the field of oncology. Inorganic nanoparticles have demonstrated successes in imaging and treatment of tumors both ex vivo and in vivo, with promising achievements in clinical trials. Since, the most considerable limitations of conventional therapies and diagnostic modalities are associated with nonspecific targeting; designing intelligent new anti-cancer therapeutics improved by targeting biomolecules could enhance cellular internalization followed by enhancement of therapeutic and diagnostic efficiency of cancer cells. [1, 6, 14]

In this study two different nanoparticles, which were synthesized in this lab, were used in order to conjugate with variety of biomolecules through a simple EDC/NHS chemistry, to investigate cancer cells targeting.

Firstly, $Sr_3MgSi_2O_8:Eu^{2+}$, Dy^{3+} persistent luminescence NPs were conjugated to folic acid. Then, some characterization studies were performed in order to confirm the conjugation and investigate some of the properties of the NPs after conjugation with folic acid. In addition the conjugation procedure was optimized based on the characterization results.

The photoluminescence properties of NPs after conjugation were studied. Based on the photoluminescence results, the intensity of emission spectra of AG NPs reduced almost two times after conjugation with FA, which could be due to a quenching phenomenon which occurred because of surface defects caused during coating and conjugation steps. However, more experiments such as luminescent lifetime should be

conducted to study the luminescence properties of the FA-NPs and investigate whether energy transfer occurred or not.

UV-Vis spectrophotometer was used to confirm conjugation, as well as calculating the conjugation efficiency (28.053 µg FA per 125 µg AG-FA NPs)

Zeta potential was performed using dynamic light scattering (DLS) device to confirm the FA conjugation to NPs and the results showed that the conjugated FA-NPs were more stable than AG NPs alone in an aqueous solutions based on zeta potential values.

The size of NPs after conjugation was measured using DLS and the results showed that the size of nanoparticles decreased almost two times after NaOH soaking method (as was previously used by another group to obtain nanometer sized particles [56]) and FA conjugation. Also, filtration could be an effective way to reduce the size. Thus, the size of the AG NPs reduced from 1296.8 µm to 543.2 nm after NaOH soaking, FA conjugation and filtration by 1 µm pore size filtration paper.

Cell viability studies were conducted using MTT assay. These results clearly demonstrated that FA conjugation provide a non-toxic coating on AG NPs nanoparticles and corroborate the results as shown in the cellular uptake studies.

Lastly, fluorescent imaging of FA-NPs was done using PC-3 cells (negative for folic acid) MCF-7 (positive for folic acid) and KB cells (more positive for folic acid as compared to MCF-7 cells) to compare the cellular uptake and confirm targeted delivery. These persistent luminescence nanoparticles could be further conjugated with photosensitizer to produce singlet oxygen to kill cancer cells in targeted photodynamic therapy especially for breast cancer cells.

Also the same NPs were conjugated to cyclic RGDfK and fluorescent imaging was done using MDA-MB-231 breast cancer cell line as positive for $\alpha_v\beta_3$ integrin receptor

and MCF-7 as negative for $\alpha_v\beta_3$ integrin receptor to compare the cellular uptake and confirm targeted delivery. The main reason for choosing RGD peptide over folic acid was the more specificity of RGD peptide to breast cancer cells as compared to folic acid. The results showed that the uptake of RGD-NPs by breast cancer cell lines is integrin $\alpha_v\beta_3$ dependent.

Moreover, the ZnS:Mn luminescent NPs were used to conjugate to prostate specific membrane antigen (PSMA) inhibitor. It has been shown that inhibitors of PSMA strongly bind to PSMA expressed on prostate cancer cells. LNCaP and PC-3 cell lines were used as positive and negative for PSMA receptors in fluorescent imaging to compare the cellular uptake and confirm targeted delivery. This biomolecule could introduce new avenues for prostate cancer applications, as it is more specific to prostate cancer cells as compared to folic acid and RGD peptide.

Finally, the persistent luminescence NPs were conjugated to R11-SH peptide and Fluorescent Imaging was performed on LNCaP and PC-3 cells as models for prostate cancer cell lines and the uptake of AG NPs alone and R11-NPs were studied. Higher uptake for conjugated R11-NPs was observed as compared to NPs alone. Also there might be a higher uptake for LNCaP cells as compared to PC-3 cells according to other data related to different sections of the samples under the microscope. Other studies also demonstrated that oligoarginine peptide (i.e., R11) appears to have high affinity to prostate cancer cells compared with other peptides tested.

Consequently, based on all the results related to different biomolecules, cellular uptake and targeting of luminescent NPs could be enhanced, by conjugation to variety of biomolecules which are specific for breast and prostate cancer (second cause of death among women and men in United States [39]) and it was also shown that the cellular uptake is receptor dependent. Thus, for prostate cancer targeting either PSMA inhibitor

or R11 peptide could be the best candidates because of their higher specificity for prostate cancer cell receptors. Since, PSMA is not only overexpressed on the surface of prostate cancers but also on the neovasculature of all solid tumors, this targeting strategy has attracted much attention for therapy and diagnosis applications. However, for breast cancer targeting RGD peptide is highly recommended as it is more specific than folic acid. Although there are still some challenges related to nonspecific adhesion of RGD peptide, since $\alpha_v\beta_3$ integrin is also expressed on normal tissue and non-cancerous inflamed tissues, development of phage display screening methods could successfully isolate peptide ligands with high specificity and affinity to various targets. Also, It was shown that cyclic RGD penta-peptide analogs such as c(RGDfK), which was also used in this project, is a promising candidate due to its high receptor binding affinity and specificity. [41, 42] In addition, folic acid could be used to target variety of cancer cells including breast, ovaries, endometrium, renal cell carcinoma, lungs, kidneys, colon, brain metastases, colorectal, and neuroendocrine carcinoma due to their enhanced mitosis rates. However, since folate receptors are expressed not only in tumor tissue but also in normal epithelia in the choroids plexus, placenta, lung, intestine, and kidney, these nanoparticulate systems should be further studied to increase tumor selectivity. [90]

4.2 Future works

In this study, the goal was to qualitatively investigate the cellular uptake of different nanoparticles conjugated to variety of biomolecules. However quantitative studies could be further performed in the future to confirm the results in this project.

In addition, since all the results were done in vitro, in vivo studies could be further considered in order to reach the point to use these designed nanoparticulate systems in several biomedical applications.

References

1. Huang, Huang-Chiao, et al. "Inorganic nanoparticles for cancer imaging and therapy." *Journal of Controlled Release* 155.3 (2011): 344-357.

2. Bharali, Dhruba J., and Shaker A. Mousa. "Emerging nanomedicines for early cancer detection and improved treatment: current perspective and future promise." *Pharmacology & therapeutics* 128.2 (2010): 324-335.

3. Levenson, Victor V. "Biomarkers for early detection of breast cancer: what, when, and where?." *Biochimica et Biophysica Acta (BBA)-General Subjects*1770.6 (2007): 847-856.

4. Chen, Hongmin, et al. "Nanoparticles for improving cancer diagnosis." *Materials Science and Engineering: R: Reports* (2013).

5. Chidambaram, Moorthi, R. Manavalan, and K. Kathiresan. "Nanotherapeutics to overcome conventional cancer chemotherapy limitations." *Journal of Pharmacy & Pharmaceutical Sciences* 14.1 (2011): 67-77.

6. Wadajkar, Aniket S., et al. "Prostate cancer-specific thermo-responsive polymer-coated iron oxide nanoparticles." *Biomaterials* (2013).

7. Juzenas, Petras, et al. "Quantum dots and nanoparticles for photodynamic and radiation therapies of cancer." *Advanced drug delivery reviews* 60.15 (2008): 1600-1614.

8. Chatterjee, Dev Kumar, Li Shan Fong, and Yong Zhang. "Nanoparticles in photodynamic therapy: an emerging paradigm." *Advanced drug delivery reviews*60.15 (2008): 1627-1637.

9. Dykman, Lev, and Nikolai Khlebtsov. "Gold nanoparticles in biomedical applications: recent advances and perspectives." *Chemical Society Reviews*41.6 (2012): 2256-2282.

10. Cheng, Yu, et al. "Highly efficient drug delivery with gold nanoparticle vectors for in vivo photodynamic therapy of cancer." *Journal of the American Chemical Society* 130.32 (2008): 10643-10647.

11. Olivo, Malini, et al. "Targeted therapy of cancer using photodynamic therapy in combination with multi-faceted anti-tumor modalities." *Pharmaceuticals* 3.5 (2010): 1507-1529.

12. Danhier, Fabienne, Olivier Feron, and Véronique Préat. "To exploit the tumor microenvironment: Passive and active tumor targeting of nanocarriers for anti-cancer drug delivery." *Journal of Controlled Release* 148.2 (2010): 135-146.

13. Brannon-Peppas, Lisa, and James O. Blanchette. "Nanoparticle and targeted systems for cancer therapy." *Advanced drug delivery reviews* (2012).

14. Gu, Frank X., et al. "Targeted nanoparticles for cancer therapy." *Nano today* 2.3 (2007): 14-21.

15. Antidiabetics, Oral. "Handbook of Experimental Pharmacology."

16. Zhou, Jian, et al. "Analysis of oligo-arginine cell-permeable peptides uptake by prostate cells." *Amino acids* 42.4 (2012): 1253-1260.

17. Karra, Nour, and Simon Benita. "The ligand nanoparticle conjugation approach for targeted cancer therapy." *Current drug metabolism* 13.1 (2012): 22-41.

18. Sabbagh Alvani, A.A et al. “Effects of dopant concentrations on phosphorescence properties of Eu/Dy-doped $Sr_3MgSi_2O_8$.” *Journal of Luminescence 114 (2005) 131–136*

19. Pan, Wen et al. “A Novel Synthesis of Alkaline Earth Silicate Phosphor $Sr_3MgSi_2O_8$:Eu^{2+},Dy^{3+}.” *Chinese Journal of Chemistry, 2007, 25, 605—608*

20. Homayoni, Homa. “Protoporphyrin IX (PpIX) -Conjugated Self-Lighting Nanoparticles for Photodynamic Therapy: Synthesis and Characterization.” 2013.

21. Ma, Lun, and Wei Chen. "ZnS: Cu, Co water-soluble afterglow nanoparticles: synthesis, luminescence and potential applications." *Nanotechnology* 21.38 (2010): 385604.

22. Chen, Wei. "Nanoparticle self-lighting photodynamic therapy for cancer treatment." *Journal of Biomedical Nanotechnology* 4.4 (2008): 369-376.

23. Chen, Wei, and Jun Zhang. "Using nanoparticles to enable simultaneous radiation and photodynamic therapies for cancer treatment." *Journal of nanoscience and nanotechnology* 6.4 (2006): 1159-1166.

24. Wang, Li, et al. "Tumor cell apoptosis induced by nanoparticle conjugate in combination with radiation therapy." *Nanotechnology* 21.47 (2010): 475103.

25. Manzoor, Koyakutty, et al. "Bio-conjugated luminescent quantum dots of doped ZnS: a cyto-friendly system for targeted cancer imaging." *Nanotechnology* 20.6 (2009): 065102.

26. Mohagheghpour, E., et al. "Controllable synthesis, characterization and optical properties of ZnS: Mn nanoparticles as a novel biosensor." *Materials Science and Engineering: C* 29.6 (2009): 1842-1848.

27. Geszke, Malgorzata, et al. "Folic acid-conjugated core/shell ZnS: Mn/ZnS quantum dots as targeted probes for two photon fluorescence imaging of cancer cells." *Acta biomaterialia* 7.3 (2011): 1327-1338.

28. Lee, Dong Won, et al. "High-resolution three-photon biomedical imaging using doped ZnS nanocrystals." (2013).

29. Ma, Lun. "The Synthesis, Optical Properties And Biological Applications Of Mn^{2+}, Cu^{2+} And Ag^{+} Doped Zns Nanoparticles." (2011).

30. Dutta, Ranu K., Prashant K. Sharma, and Avinash C. Pandey. "Design and surface modification of potential luminomagnetic nanocarriers for biomedical applications." *Journal of nanoparticle research* 12.4 (2010): 1211-1219.

31. Xiong, Li-Qin, et al. "Synthesis, characterization, and in vivo targeted imaging of amine-functionalized rare-earth up-converting nanophosphors."*Biomaterials* 30.29 (2009): 5592-5600.

32. Zhou, Jing, et al. "A versatile fabrication of upconversion nanophosphors with functional-surface tunable ligands." *Journal of Materials Chemistry* 20.37 (2010): 8078-8085.

33. Blanco, M. Dolores, et al. "In vitro and in vivo evaluation of a folate-targeted copolymeric submicrohydrogel based on n-isopropylacrylamide as 5-Fluorouracil delivery system." *Polymers* 3.3 (2011): 1107-1125.

34. Pi, Jiang, et al. "Pathway of cytotoxicity induced by folic acid modified selenium nanoparticles in MCF-7 cells." *Applied microbiology and biotechnology* 97.3 (2013): 1051-1062.

35. Hattori, Yoshiyuki, and Yoshie Maitani. "Folate-linked lipid-based nanoparticle for targeted gene delivery." *Current drug delivery* 2.3 (2005): 243-252.

36. Pan, Jie, and Si-Shen Feng. "Targeting and imaging cancer cells by folate-decorated, quantum dots (QDs)-loaded nanoparticles of biodegradable polymers." *Biomaterials* 30.6 (2009): 1176-1183.

37. Retnakumari, Archana, et al. "Molecular-receptor-specific, non-toxic, near-infrared-emitting Au cluster-protein nanoconjugates for targeted cancer imaging." *Nanotechnology* 21.5 (2010): 055103.

38. Liu, Yanhua, et al. "Dual targeting folate-conjugated hyaluronic acid polymeric micelles for paclitaxel delivery." *International journal of pharmaceutics* 421.1 (2011): 160-169.

39. Siegel, Rebecca, Deepa Naishadham, and Ahmedin Jemal. "Cancer statistics, 2012." *CA: a cancer journal for clinicians* 62.1 (2012): 10-29.

40. Yang, Wanhua, et al. "Inhibition of proliferative and invasive capacities of breast cancer cells by arginine-glycine-aspartic acid peptide in vitro." *Oncology reports*15.1 (2006): 113-117.

41. Ye, Yunpeng, and Xiaoyuan Chen. "Integrin targeting for tumor optical imaging."*Theranostics* 1 (2011): 102.

42. Wang, Zhe, Wai-Keung Chui, and Paul C. Ho. "Design of a multifunctional PLGA nanoparticulate drug delivery system: evaluation of its physicochemical properties and anticancer activity to malignant cancer cells." *Pharmaceutical research* 26.5 (2009): 1162-1171.

43. Cai, Weibo, et al. "Peptide-labeled near-infrared quantum dots for imaging tumor vasculature in living subjects." *Nano letters* 6.4 (2006): 669-676.

44. Valencia, Pedro M., et al. "Effects of ligands with different water solubilities on self-assembly and properties of targeted nanoparticles." *Biomaterials* 32.26 (2011): 6226-6233.

45. Wang, Fen, et al. "The Functions and Applications of RGD in Tumor Therapy and Tissue Engineering." *International journal of molecular sciences* 14.7 (2013): 13447-13462.

46. Dhar, Shanta, et al. "Targeted delivery of cisplatin to prostate cancer cells by aptamer functionalized Pt (IV) prodrug-PLGA–PEG nanoparticles." *Proceedings of the National Academy of Sciences* 105.45 (2008): 17356-17361.

47. Gu, Frank, et al. "Precise engineering of targeted nanoparticles by using self-assembled biointegrated block copolymers." *Proceedings of the National Academy of Sciences* 105.7 (2008): 2586-2591.

48. Farokhzad, Omid C., et al. "Targeted nanoparticle-aptamer bioconjugates for cancer chemotherapy in vivo." *Proceedings of the National Academy of Sciences* 103.16 (2006): 6315-6320.

49. Liu, Tiancheng, et al. "Cell-Surface labeling and internalization by a fluorescent inhibitor of prostate-specific membrane antigen." *The Prostate* 68.9 (2008): 955-964.

50. Mousa, Shaker A., and Dhruba J. Bharali. "Nanotechnology-based detection and targeted therapy in cancer: nano-bio paradigms and applications." *Cancers*3.3 (2011): 2888-2903.

51. LaRocque, Justin, Dhruba J. Bharali, and Shaker A. Mousa. "Cancer detection and treatment: the role of nanomedicines." *Molecular biotechnology* 42.3 (2009): 358-366.

52. Farokhzad, Omid C., et al. "Microfluidic system for studying the interaction of nanoparticles and microparticles with cells." *Analytical chemistry* 77.17 (2005): 5453-5459.

53. Farokhzad, Omid C., et al. "Nanoparticle-aptamer bioconjugates a new approach for targeting prostate cancer cells." *Cancer research* 64.21 (2004): 7668-7672.

54. Ding, Pingyu, Paul Helquist, and Marvin J. Miller. "Design, synthesis and pharmacological activity of novel enantiomerically pure phosphonic acid-based NAALADase inhibitors." *Organic & biomolecular chemistry* 5.5 (2007): 826-831.

55. Zhou, Jian, Jinhai Fan, and Jer-Tsong Hsieh. "Inhibition of mitogen-elicited signal transduction and growth in prostate cancer with a small peptide derived from the

functional domain of DOC-2/DAB2 delivered by a unique vehicle."*Cancer research* 66.18 (2006): 8954-8958.

56. Maldiney, T., D. Scherman, and C. Richard. "Persistent Luminescence Nanoparticles for Diagnostics and Imaging." *ACS Symposium Series, American Chemical Society*. Vol. 1113. 2012.
57. Durdureanu-Angheluta, A., et al. "Progress in the synthesis and characterization of magnetite nanoparticles with amino groups on the surface."*Journal of Magnetism and Magnetic Materials* 324.9 (2012): 1679-1689.
58. VOHRA, VARUN. “Multilevel organization of hybrid materials based on zeolite L crystals for light emitting devices applications.” *Diss. Università degli Studi di Milano-Bicocca*, 2009.
59. Kehr, Nermin Seda, et al. "Cell Adhesion and Cellular Patterning on a Self-Assembled Monolayer of Zeolite L Crystals." *Advanced Functional Materials*20.14 (2010): 2248-2254.
60. Yuan, Peng, et al. "Functionalization of halloysite clay nanotubes by grafting with γ-aminopropyltriethoxysilane." *The Journal of Physical Chemistry C* 112.40 (2008): 15742-15751.
61. Gao, Ruixia, et al. "Selective extraction of sulfonamides from food by use of silica-coated molecularly imprinted polymer nanospheres." *Analytical and bioanalytical chemistry* 398.1 (2010): 451-461.
62. Sunoqrot, Suhair, et al. "Temporal control over cellular targeting through hybridization of folate-targeted dendrimers and PEG-PLA nanoparticles."*Biomacromolecules* 13.4 (2012): 1223-1230.
63. Narayanan, Sreeja, et al. "Folate targeted polymeric'green'nanotherapy for cancer." *Nanotechnology* 21.28 (2010): 285107.

64. SHAN, JIANG. "Use of upconversion fluorescent nanoparticles for simultaneous imaging, detection and delivery of sirna." (2009).

65. Suriamoorthy, Preethi, et al. "Folic acid-CdTe quantum dot conjugates and their applications for cancer cell targeting." *Cancer Nanotechnology* 1.1-6 (2010): 19-28.

66. Lakshmanan, Santana Bala. "Gold/Copper Sulphide and Gold Nanoparticles for Application in Cancer Therapy." (2012).

67. Yang, Chang, et al. "Surface plasmon-enhanced Ag/CuS nanocomposites for cancer treatment." *Cancer Nanotechnology* (2013): 1-9.

68. Delaittre, Guillaume, et al. "Chemical approaches to synthetic polymer surface biofunctionalization for targeted cell adhesion using small binding motifs." *Soft Matter* 8.28 (2012): 7323-7347.

69. Hersel, Ulrich, Claudia Dahmen, and Horst Kessler. "RGD modified polymers: biomaterials for stimulated cell adhesion and beyond." *Biomaterials* 24.24 (2003): 4385-4415.

70. Wang, Zhe, Wai-Keung Chui, and Paul C. Ho. "Nanoparticulate delivery system targeted to tumor neovasculature for combined anticancer and antiangiogenesis therapy." *Pharmaceutical research* 28.3 (2011): 585-596.

71. Chen, Rui, et al. "The use of poly (l-lactide) and RGD modified microspheres as cell carriers in a flow intermittency bioreactor for tissue engineering cartilage."*Biomaterials* 27.25 (2006): 4453-4460.

72. Wang, Zhe, and Paul C. Ho. "Self-Assembled Core–Shell Vascular-Targeted Nanocapsules for Temporal Antivasculature and Anticancer Activities." *Small*6.22 (2010): 2576-2583.

73. Xue, Mei, et al. "The preparation of glutathione-capped CdTe quantum dots and their use in imaging of cells." *Talanta* 83.5 (2011): 1680-1686.

74. Ren, Yupeng, Sek Man Wong, and Lee-Yong Lim. "Folic acid-conjugated protein cages of a plant virus: a novel delivery platform for doxorubicin."*Bioconjugate chemistry* 18.3 (2007): 836-843.

75. Jain, Rishabh, et al. "The use of native chemical functional groups presented by wound beds for the covalent attachment of polymeric microcarriers of bioactive factors." *Biomaterials* (2012).

76. Hao, Guiyang, et al. "A cell permeable peptide analog as a potential-specific PET imaging probe for prostate cancer detection." *Amino acids* 41.5 (2011): 1093-1101.

77. Tyagi, Amit, and Alfons Penzkofer. "Fluorescence spectroscopic behaviour of folic acid." *Chemical Physics* 367.2 (2010): 83-92.

78. Hirakawa, Kazutaka, et al. "Sequence-specific DNA damage induced by ultraviolet A-irradiated folic acid via its photolysis product." *Archives of biochemistry and biophysics* 410.2 (2003): 261-268.

79. Majoros, István J., et al. "Methotrexate delivery via folate targeted dendrimer-based nanotherapeutic platform." *Wiley Interdisciplinary Reviews: Nanomedicine and Nanobiotechnology* 1.5 (2009): 502-510.

80. Das, Manasi, and Sanjeeb K. Sahoo. "Folate decorated dual drug loaded nanoparticle: role of curcumin in enhancing therapeutic potential of nutlin-3a by reversing multidrug resistance." *PloS one* 7.3 (2012): e32920.

81. Nune, Satish K., et al. "Green nanotechnology from tea: phytochemicals in tea as building blocks for production of biocompatible gold nanoparticles." *Journal of materials chemistry* 19.19 (2009): 2912-2920.

82. Liu, Longfei, Qingqing Miao, and Gaolin Liang. "Quantum Dots as Multifunctional Materials for Tumor Imaging and Therapy." *Materials* 6.2 (2013): 483-499.

83. Wu, Aiguo. "Biocompatible composite nanoparticles with large longitudinal relaxivity for targeted imaging and early diagnosis of cancer." *J. Mater. Chem. B*(2013).

84. Rosenholm, Jessica M., et al. "Targeting of porous hybrid silica nanoparticles to cancer cells." *ACS nano* 3.1 (2008): 197-206.

85. Mi, Yu, et al. "Multimodality treatment of cancer with herceptin conjugated, thermomagnetic iron oxides and docetaxel loaded nanoparticles of biodegradable polymers." *Biomaterials* (2012).

86. Liu, Zhuang, and Rui Peng. "Inorganic nanomaterials for tumor angiogenesis imaging." *European journal of nuclear medicine and molecular imaging* 37.1 (2010): 147-163.

87. Ferro-Flores, G., et al. "Peptides for in vivo target-specific cancer imaging." *Mini Reviews in Medicinal Chemistry* 10.1 (2010): 87-97.

88. Zako, Tamotsu, et al. "Cyclic RGD peptide-labeled upconversion nanophosphors for tumor cell-targeted imaging." *Biochemical and biophysical research communications* 381.1 (2009): 54-58.

89. Patel, Ronak H., et al. "Multifunctionality of indocyanine green-loaded biodegradable nanoparticles for enhanced optical imaging and hyperthermia intervention of cancer." *Journal of Biomedical Optics* 17.4 (2012): 0460031-04600310.

90. Kamaly, Nazila, et al. "Targeted polymeric therapeutic nanoparticles: design, development and clinical translation." *Chemical Society Reviews* 41.7 (2012): 2971-3010.

Biographical Information

Leila Hossein Rashidi was born in Tehran, Iran in April 1988. She graduated with a Bachelor's degree in Textile Engineering (Chemistry and Fiber Science) from Amirkabir University of Technology, Iran in August 2010.

To accomplish her goal aimed at a future in medical based research and clinical frontier, she joined the University of Texas at Arlington in fall 2011, focused on achieving a graduate degree in Biomedical Engineering. She began her research study in the Nano-Bio Physics lab as a research assistant under supervision of Professor Wei Chen, whose expertise is in the field of nanotechnology, biomaterials and cancer diagnosis and treatment based on luminescent nanoparticulate systems. She worked on several projects encompassing those related with synthesis, characterization, conjugation and targeting.

Her research interests include drug delivery, biomaterials, nanotechnology and their application in cancer diagnosis and treatment. Her future plan is to continue a career encompassing applications of nanobiomaterials in cancer diagnosis and treatment.